

### Cryo-EM reveals open and closed Asgard chromatin assemblies

Ranawat, H.M.; Cajili, M.K.; Lopez-Barbosa, N.; Quail, T.; Dame, R.T.; Dodonova, S.O.

#### Citation

Ranawat, H. M., Cajili, M. K., Lopez-Barbosa, N., Quail, T., Dame, R. T., & Dodonova, S. O. (2025). Cryo-EM reveals open and closed Asgard chromatin assemblies. *Molecular Cell*, 85, 1-14. doi:10.1016/j.molcel.2025.10.001

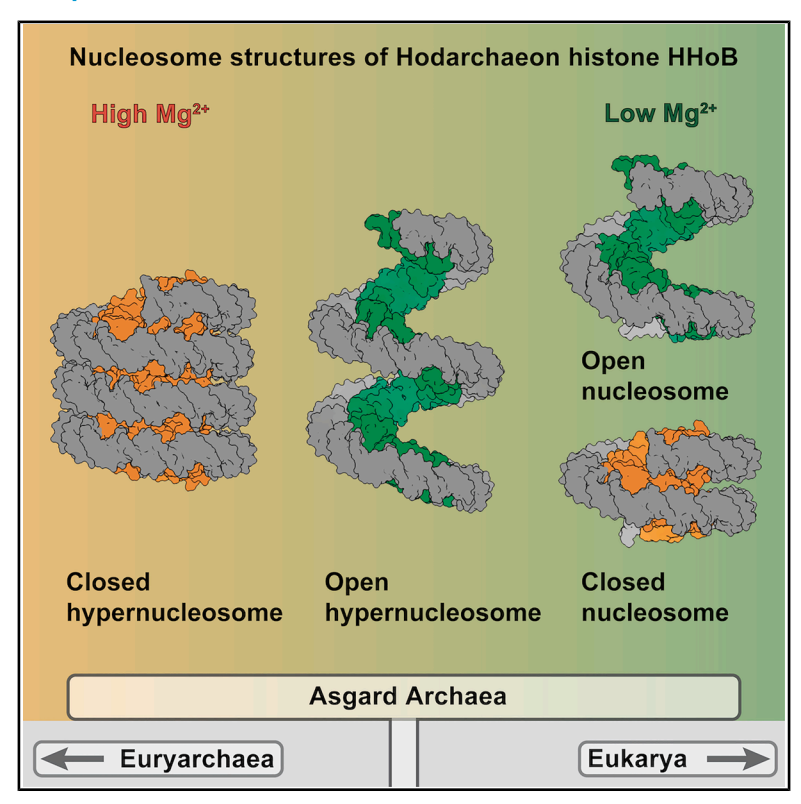
Version: Corrected Publisher's Version

License: <u>Creative Commons CC BY 4.0 license</u>
Downloaded from: <u>https://hdl.handle.net/1887/4281705</u>

**Note:** To cite this publication please use the final published version (if applicable).

# Cryo-EM reveals open and closed Asgard chromatin assemblies

### **Graphical abstract**



#### **Authors**

Harsh M. Ranawat, Marc K. Cajili, Natalia Lopez-Barbosa, Thomas Quail, Remus T. Dame, Svetlana O. Dodonova

#### Correspondence

svetlana.dodonova@embl.de

#### In brief

Ranawat et al. show the cryo-EM structures of Asgard archaeal chromatin assemblies, revealing that the histone HHoB assembles into both compact closed and extended open hypernucleosomes. The closed conformation is conserved across archaea, while the open conformation represents an Asgard-specific innovation.

#### **Highlights**

- Cryo-EM reveals chromatin assemblies formed by Asgard histone HHoB
- HHoB histone forms both compact closed and extended open hypernucleosomes
- Closed hypernucleosomes are conserved among archaea;
   open hypernucleosomes are Asgard-specific
- Mg<sup>2+</sup> ions regulate the balance between open and closed chromatin states





#### **Article**

# **Cryo-EM reveals open and closed Asgard chromatin assemblies**

Harsh M. Ranawat, <sup>1,2</sup> Marc K. Cajili, <sup>3</sup> Natalia Lopez-Barbosa, <sup>4</sup> Thomas Quail, <sup>4</sup> Remus T. Dame, <sup>3</sup> and Svetlana O. Dodonova<sup>1,5,\*</sup>

<sup>1</sup>Molecular Systems Biology Unit, European Molecular Biology Laboratory (EMBL), Meyerhofstrasse 1, 69117 Heidelberg, Germany <sup>2</sup>Collaboration for joint PhD degree between EMBL and Heidelberg University, Faculty of Biosciences, 69120 Heidelberg, Germany

#### **SUMMARY**

Asgards are the closest archaeal relatives of eukaryotes, representing an important step in chromatin evolution. However, their chromatin organization has remained enigmatic until now. In this study, we present the first structures of Asgard chromatin assemblies formed by the Hodarchaeal histone HHoB. Our high-resolution cryo-electron microscopy (cryo-EM) structures reveal that this Asgard histone assembles into compact "closed" and into extended "open" hypernucleosomes. Thus, the closed hypernucleosome conformation is conserved across archaeal lineages, while the open conformation resembles a eukaryotic H3–H4 octasome and likely represents an Asgard-specific innovation. Moreover, we show that Mg²+ ions influence Asgard chromatin conformation, suggesting a regulatory role. Overall, our study provides the first structure-based model of Asgard chromatin organization, expanding our understanding of chromatin architecture in an evolutionary context.

#### **INTRODUCTION**

Eukaryotes and most archaea use histone proteins to organize their genomes and regulate chromatin states. In eukaryotes, a histone octamer wraps 147 bp of DNA into a nucleosome. The histone fold domain and dimer "handshake" motif are conserved across the tree of life, 2,3 and it is widely accepted that the eukaryotic histones trace their lineage to archaeal histones.<sup>4</sup> The histone fold is composed of three  $\alpha$  helices ( $\alpha$ 1,  $\alpha$ 2, and  $\alpha$ 3) linked by short loops L1 and L2. During dimerization, the L1 loop of one histone pairs with the L2 loop of its partner, creating the handshake motif.<sup>5</sup> However, while eukaryotic core histones form obligate heterodimers (H2A-H2B, H3-H4), archaeal histones can form both homodimers and heterodimers. 6 Furthermore, instead of forming nucleosomes of a defined size (~147 bp) wrapped by a histone octamer, archaeal histones assemble into histone-DNA complexes nucleosomes of variable size (N  $\times$  30 bp), where N histone dimers can each wrap 30 bp of DNA.7,8 Notably, most archaeal histones lack extended tails that are hallmarks of eukaryotic histones.9 Eukaryotic histones can be substituted by different variants, 10 can form sub-nucleosomal particles, 11 and noncanonical nucleosomes like a H3-H4 octasome<sup>12</sup>; but generally, the nucleosomal core structure is highly conserved and has been extensively studied. 1,13

Our understanding of archaeal chromatin is based on a few model species from the Euryarchaeota, such as *Methanother*-

mus fervidus and Thermococcus kodakarensis. The first pivotal study on archaeal chromatin structure revealed a 90-bp nucleosome formed by the tail-less histone HMfB from M. fervidus.7 Here, we use "nucleosome" to describe any archaeal histone-DNA complex and "hypernucleosome" for assemblies with more than two superhelical turns. Interestingly, the crystal packing of the HMfB-DNA structure suggested a continuous, tightly packed hypernucleosome with strong stacking interactions between histones,9 later supported via biophysical approaches. 14 A cryo-electron microscopy (cryo-EM) study of the related histone HTkA from T. kodakarensis confirmed this structure and revealed an additional "slinkie-like" configuration, 15 where, a 90-bp nucleosome was connected via a short DNA linker to a 120-bp nucleosome, while the arrangement of histones within these nucleosomes remained consistent with the HMfB-based structure. This study demonstrated that archaeal chromatin exhibits greater conformational diversity than previously recognized.

Although Euryarchaeota provided early insights into archaeal chromatin, many other archaeal groups remain understudied, which limits our understanding of archaeal chromatin architecture. The recently discovered Asgard superphylum of archaea presents particularly intriguing chromatin features, based on metagenomic analyses. <sup>16</sup> Many Asgard metagenomes encode multiple histone variants, some of which include extended histone tails. <sup>9</sup> For instance, the Asgard metagenome of Hodarchaeales LC3

<sup>&</sup>lt;sup>3</sup>Leiden Institute of Chemistry, Leiden University, Einsteinweg 55, 2333 CC Leiden, the Netherlands

<sup>&</sup>lt;sup>4</sup>Cell Biology and Biophysics Unit, EMBL, Meyerhofstrasse 1, 69117 Heidelberg, Germany

<sup>&</sup>lt;sup>5</sup>Lead contact

<sup>\*</sup>Correspondence: svetlana.dodonova@embl.de https://doi.org/10.1016/j.molcel.2025.10.001



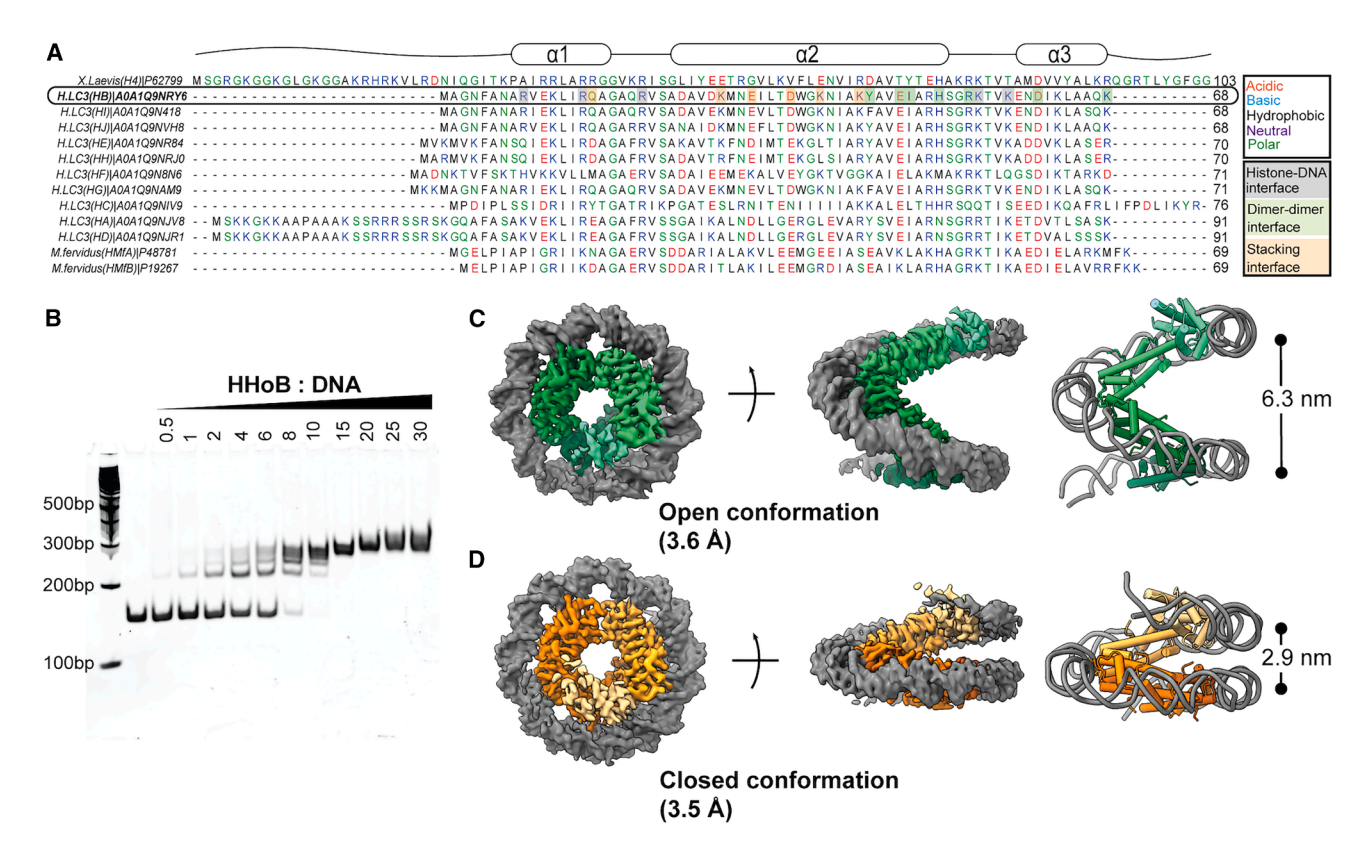


Figure 1. Cryo-EM structures of HHoB nucleosomes in open and closed states

(A) Sequence alignment of LC3 Asgard, M. fervidus, and human H4 histones. Residues at DNA-histone (gray), dimer-dimer (green), and stacking (orange) interfaces are highlighted.

- (B) EMSA of 147 bp Widom601 DNA with increasing HHoB ratios.
- (C) Cryo-EM map and model of the open HHoB-DNA complex in 1 mM MgCl<sub>2</sub>. DNA is gray, and histone dimers are green.
- (D) Cryo-EM map and model of the closed HHoB-DNA complex in 1 mM MgCl<sub>2</sub>. DNA is gray, and histone dimers are orange.

(previously Candidatus Heimdallarchaeota LC3<sup>17</sup>) encodes ten histones: eight short tail-less histones and two histones with extended tails. 9,16 Asgard archaea typically possess larger genomes and encode eukaryotic signature proteins. 17 It is widely accepted that eukaryotes originated from within the Asgard superphylum, 17-19 inheriting much of their "information processing" machinery from archaea. Consequently, Asgard histones represent a critical step in chromatin evolution, leading toward eukaryotic chromatin or to viral histones as an intermediate step. 16,20,21

In this study, we provide the first insights into the structure and function of Asgard chromatin assemblies. We structurally, biochemically, and biophysically characterize chromatin assemblies formed by a tail-less histone (HHoB) from the Asgard archaea Hodarchaeales LC3. We present several high-resolution cryo-EM structures of nucleosomes formed by the HHoB histone wrapping DNA. Our structures reveal that the HHoB histone forms two distinct nucleosomal conformations—closed and open—under a wide range of conditions. We demonstrate that increasing Mg²+ concentrations favor the formation of continuous hypernucleosomes, and we report cryo-EM structures of both closed and open hypernucleosomes. The ability of Asgard histones to form closed hypernucleosomes experimentally con-

firms that this chromatin state is conserved across distant archaeal groups such as Euryarchaeota and Asgards. By contrast, the novel open chromatin state has not been observed previously and may represent an Asgard-specific innovation. Overall, our study provides the first structural insights into Asgard chromatin organization, expanding our understanding of archaeal chromatin architecture. These findings are validated through mutagenesis, biochemical assays, and single-molecule biophysical experiments.

#### **RESULTS**

# Asgard histone HHoB forms open and closed nucleosomes in vitro

The LC3 Asgard genome encodes ten histone proteins, the majority of which (eight) are short histones lacking extended tails (Figure 1A). First, three of the short histones (HHoB, 68 amino acids; HHoF, 71; and HHoG, 71) were selected for initial biochemical analysis (Figure 1A). Each histone was recombinantly expressed and purified. Archaeal nucleosomes were then reconstituted *in vitro* by incubating Widom601 147-bp DNA with each histone in buffer A (20 mM HEPES pH 7.5, 100 mM NaCl). Widom601<sup>22</sup> is an artificial DNA sequence that

### **Article**



was engineered for its ability to position eukaryotic histone octamers, that form stable nucleosomes, and that has been used in the majority of eukaryotic nucleosome structural studies<sup>23,24</sup> and in the latest study of HTkA archaeal nucleosomes. 15 Therefore, we used the Widom601 DNA to allow direct comparison with other structures. All three histones exhibited similar DNA binding behavior in electrophoretic mobility shift assays (EMSAs) and demonstrated a comparable range of binding affinities (Figures 1B and S1). For HHoB, the affinity is  $30.8 \pm 3.7$  nM (mean  $\pm$  standard deviation, n = 3) as measured by microscale thermophoresis (MST) (Figure S2). Unlike the well-studied histone HMfB from M. fervidus, which displays highly cooperative binding behavior reflected in a single shifted band,<sup>25</sup> the HHoB, HHoF, and HHoG histones exhibited a ladder-like binding pattern (Figures 1B and S1). Based on the similar behavior of these three Asgard histones, we proceeded with a more in-depth analysis of the HHoB histone.

Mg2+ ions are essential and abundant in eukaryotic cells (1-10 mM<sup>26,27</sup>) and in archaeal cells (120 mM in Euryarchaea<sup>28</sup>), and they are known to modulate chromatin structure in bacteria.<sup>29,30</sup> However, as Asgard archaea are extremely difficult to isolate and cultivate, 31,32 we lack the data on their intracellular ion concentration and can only assume that the physiological range is anywhere between the known ranges for archaea, bacteria, and eukaryotes (1-120 mM). Notably, samples used in all structural studies in the field have also contained Mg<sup>2+</sup>. 7,15 Therefore, we reconstituted the HHoB-based Asgard nucleosomes in buffer A supplemented with 1 mM Mg2+, where the concentration of 1 mM was chosen as minimally physiologically relevant. The samples were incubated at room temperature (RT) for 20 min, plunge-frozen, and subjected to cryo-EM singleparticle analysis (SPA). From the collected particles, after 2D and 3D classification in cryoSPARC,33 two main 3D classes emerged, revealing two distinct conformations that we refer to as closed and open (Figures 1C and 1D). In the closed conformation histone dimers wrap the DNA into a tightly packed superhelix and make extensive stacking contacts with each other (interactions between dimers N and N+2, N and N+3). In the open conformation, the histones wrap the DNA into a much more extended open superhelix with a large distance between turns and absence of stacking interactions between histones (Figures 1C and 1D). Both classes were equally abundant in the dataset (34.7% and 42.4%) along with some "low-quality" classes that were filtered out (Figure S3). The two main classes were refined to 3.4 and 3.6 Å resolution, respectively (Figure S3; Table 1; Video S1), and the corresponding molecular models were built using Phenix<sup>34</sup>, Coot,<sup>35</sup> and ISOLDE<sup>36</sup> (STAR

Each of the cryo-EM maps reveals a left-handed nucleosome superhelix (Figures 1C and 1D) with four HHoB histone dimers bound to 120 bp of the DNA (out of 147 bp total), consistent with the expected 30-bp footprint of a histone dimer. We note that in both EM maps, at higher density visualization thresholds, we also observed the fifth HHoB dimer bound to the DNA, albeit at lower local resolution likely caused by higher flexibility of the DNA end, typical for dynamic nucleosomal complexes<sup>24</sup> (Figure S3A). Binding of five histone dimers corresponds well to the number of shifts observed in the EMSA assays—where

binding of each dimer leads to appearance of a shifted band (Figure 1B). Binding of five histone dimers also shows that the Widom601 sequence does not have any positioning effect on the HHoB, and its positioning is simply defined by the length of the available DNA. The footprint of a histone dimer was further verified via EMSA with DNA templates of different lengths (Figure S2B).

The closed nucleosome conformation is similar to the previously reported HMfB Euryarchaeal nucleosome  $^7$  (root-mean-square deviation [RMSD] 1.1 Å between C $\alpha$  atoms), while the open conformation is novel and significantly less compacted than the closed conformation (Figures 1C and 1D). The pitch of the closed nucleosome is 29.5 Å (measured between DNA atoms N1 of A30 and N3 of T105), whereas the pitch of the open nucleosome is almost twice as wide at 63.0 Å (measured between DNA atoms N1 of A30 and N3 of A103).

# Open and closed HHoB nucleosomes coexist in a range of Mg<sup>2+</sup> conditions and form hypernucleosomes

We investigated the influence of increasing Mg<sup>2+</sup> concentrations on Asgard nucleosome structure, as Mg<sup>2+</sup> plays a crucial role in chromatin structure and dynamics regulation in both archaea and eukaryotes.<sup>37,38</sup> Based on reported physiological ranges of intracellular Mg2+ concentration in archaea,28 we reconstituted Asgard HHoB nucleosomes in the presence of 0-100 mM Mg<sup>2+</sup> in buffer A (STAR Methods). Each sample was incubated at RT for 20 min, plunge-frozen, and examined by cryo-EM (Figure S4). For each Mg2+ concentration (0, 1, 20, 40, 60, 80, and 100 mM), at least 30 micrographs were collected. First, we chose the 40-mM dataset that contained all types of particles-open, closed, and mixed (combination of stacking open and closed particles) (Figure 2A). Next, after preprocessing, we trained a Topaz<sup>39</sup> model to pick particles in the dataset. This model was then used to pick particles from all datasets (with different Mg conditions). Next, "low-quality" particles (damaged particles, ice contamination, etc.) were removed by 2D classification and sorting. We visualized and calculated the number of open, closed, or mixed 2D classes based on the helical pitch (Figure 2). Both closed and open nucleosomes were observed across a wide range of Mg<sup>2+</sup> concentrations (1-60 mM) (Figure 2A). At higher Mg2+ concentrations (80 and 100 mM), only closed nucleosomes were observed (Figure 2), while in the absence of Mg2+, only open nucleosomes were detected. We never observed chromatin aggregation or precipitation even at the highest tested Mg<sup>2+</sup> concentrations (100 mM), whereas eukaryotic chromatin is known to precipitate at very low Mg<sup>2+</sup> concentrations (5 mM).<sup>15</sup> This property may be crucial for archaea that can have up to 120 mM intracellular Mg<sup>2+</sup> concentrations.

Interestingly, even at low Mg<sup>2+</sup> concentrations (1 and 20 mM), individual nucleosomes stacked with each other to form extended hypernucleosomes (Figure 2A). These hypernucleosomes appeared in various configurations: open, closed, or mixed. With increasing Mg<sup>2+</sup> concentration, hypernucleosomes of increasing length were formed (Figure S4). The hypernucleosomes exhibited very regular arrangement and spacing and were consistently straight. The spacing (superhelical pitch) in the closed hypernucleosomes was 24.6 Å, and it was 63 Å in



Table 1. Cryo-EM data collection, refinement, and validation statistics						
Histone HHoB + 147 bp Wid601	Open nucleosome (0 mM Mg <sup>2+</sup> ) EMDB-53390 N/A	Open nucleosome (1 mM Mg <sup>2+</sup> ) EMDB-53388 PDB: 9QV7	Closed nucleosome (1 mM Mg <sup>2+</sup> ) EMDB-53386 PDB: 9QV5	Open hypernucleosome (20 mM Mg <sup>2+</sup> ) EMDB-53389 N/A	Closed hypernucleosome (100 mM Mg <sup>2+</sup> ) EMDB-53387 PDB: 9QV6	
Concentration of MgCl2 in buffer	0	1 mM	1 mM	20 mM	100 mM	
Data collection and processing	N/A	N/A	N/A	N/A	N/A	
Magnification	130,000	165,000	165,000	105,000	130,000	
Voltage (kV)	300	300	300	300	300	
Electron exposure (e-/Ų)	46.63	59.44	59.44	63.84	39.93	
Defocus range (μm)	−1.5 to −2.5	-0.5 to $-1.75$	-0.5 to $-1.75$	-0.5 to $-1.75$	−0.5 to −1.5	
Pixel size (Å)	1.04	0.73	0.73	0.82	0.645	
Symmetry imposed	C1	C1	C1	C1	C1	
Initial particle images (no.)	318,063	3,108,514	3,108,514	214,840	4,964,843	
Final particle images (no.)	96,361	96,738	117,260	40,918	3,53,468	
Map resolution (Å)	4.4	3.6	3.5	10.5	2.6	
FSC threshold	0.143	0.143	0.143	0.143	0.143	
Map resolution range (Å)	2–6	2.5-7.5	2.5–7.5	8–16	2–4	
Refinement	N/A	N/A	N/A	N/A	N/A	
Map: Model resolution (Å)	N/A	4	3.9	N/A	2.9	
FSC threshold	N/A	0.5	0.5	N/A	0.5	
Map sharpening B factor (Ų)	N/A	-50	-50	N/A	-50	
Model composition	N/A	N/A	N/A	N/A	N/A	
Non-hydrogen atoms	N/A	8,628	8,628	N/A	13,932	
Protein residues	N/A	544	544	N/A	852	
<i>B</i> factors (Ų)	N/A	N/A	N/A	N/A	N/A	
Protein	N/A	128.6	82.74	N/A	65.36	
RMSD	N/A	N/A	N/A	N/A	N/A	
Bond lengths (Å)	N/A	0.013	0.012	N/A	0.012	
Bond angles (°)	N/A	1.872	1.672	N/A	1.911	
Validation	N/A	N/A	N/A	N/A	N/A	
MolProbity score	N/A	0.81	1.42	N/A	0.91	
Clashscore	N/A	1.08	7.73	N/A	1.62	
Poor rotamers (%)	N/A	0.96	0.64	N/A	0	
Ramachandran plot	N/A	N/A	N/A	N/A	N/A	
Favored (%)	N/A	99.62	98.48	N/A	100	
Allowed (%)	N/A	0.38	1.52	N/A	0	
Disallowed (%)	N/A	0	0	N/A	0	

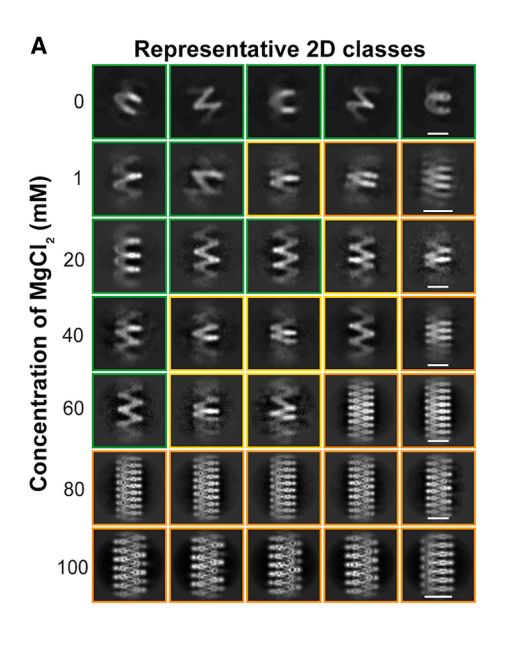
the open hypernucleosomes, consistent with the spacing of individual nucleosomes in the 1 mM Mg $^{2+}$  condition. The pitch of the closed hypernucleosome was smaller (24.6 Å) than in the individual closed nucleosomes (29.5 Å), where the DNA ends are more flexible, as they are not packed into a rigid hyper-assembly. EMSA performed at 10 mM Mg $^{2+}$  concentrations confirmed that the cooperativity of HHoB binding to DNA increased, and instead of the ladder-like shifts in EMSA, HHoB binding resulted in a single shifted band similar to HMfB (Figure S1). Histones HHoF and HHoG exhibited the same behavior (Figure S1).

Hypernucleosome formation is likely mediated by Mg<sup>2+</sup> ions binding to the negatively charged phosphate DNA backbone in a non-site-specific manner, as we could reproduce the effect

of hypernucleosome formation in the "high Mg" (100 mM) condition by substituting  $Mg^{2*}$  with other divalent cations— $Zn^{2*}$  and  $Ca^{2*}$  (Figure S5)—and as we did not observe any defined coordinated binding sites in the density (although the high resolution would allow us to resolve such sites). We note that  $Mg^{2*}$  is the most abundant divalent ion in the cells,  $^{40}$  with concentrations typically 100–1,000 times higher than  $Ca^{2*}$  or  $Zn^{2*}$ ; thus, influence of other divalent cations compared with  $Mg^{2*}$  would be negligible in native conditions.

We then tested complete absence of Mg<sup>2+</sup> ions during nucleosome reconstitution and acquired a cryo-EM dataset in the zero Mg<sup>2+</sup> condition. SPA revealed nucleosomes exclusively in the open conformation (Figure S6; Video S1). In this condition, all





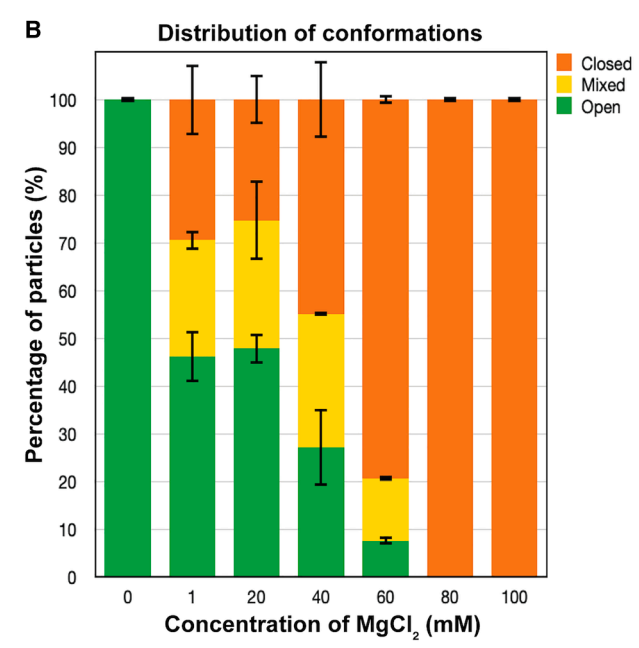


Figure 2. Effect of MgCl<sub>2</sub> on HHoB-DNA conformations
(A) Representative 2D classes: open (green), mixed (yellow), closed (orange). Scale bar, 10 nm.

(B) Distribution of conformations across datasets. Error bars: technical duplicates.

nucleosomes existed as individual particles, and formation of hypernucleosomes was not observed.

# Cryo-EM analysis reveals the structures of the closed and open HHoB hypernucleosomes

To determine the molecular structure of the closed hypernucleosome, we collected a large cryo-EM dataset on the 100 mM Mg<sup>2+</sup> sample, where 100% of particles were in the closed conformation. Closed hypernucleosomes formed true helical structures. which were processed accordingly in cryoSPARC (Figure S7). We resolved the map at 2.6 Å resolution (Figures 3B and S7; Table 1; Video S1). The high resolution allowed us to place side chains with high confidence during model building. The closed hypernucleosome structure is similar to the HMfB hypernucleosome<sup>7</sup> (RMSD of 0.8 Å over 3 histone dimers at  $C\alpha$  atoms). Closed conformations from the 1 and 100 mM conditions were very similar (RMSD 0.9 Å over 3 histone dimers at  $C\alpha$  atoms). HHoB dimers are continuously bound to the DNA, wrapping it into a tight left-handed superhelix. Individual DNA molecules (147 bp) within the assembly are "seamlessly" connected via DNA end-to-end contacts, and the histone dimers are continuously bound to the DNA with a footprint of  $\sim$ 30 bp.

Next, we collected a cryo-EM dataset on the 20 mM Mg<sup>2+</sup> condition sample to enrich for the open hypernucleosome state. The open hypernucleosomes exhibited greater flexibility, compared with the closed state, and consequently, they were resolved at a lower resolution of ~10 Å (Figures 3C, 3D, and S8; Video S1). The open hypernucleosome conformation is similar to the individual open nucleosome conformation from the 1 mM condition. We fitted the open nucleosome model built from our 3.6 Å map (1 mM condition) as a rigid body into the open hypernucleosome map

with high confidence (Figure 3D). In both open and closed hypernucleosomes, the DNA ends interact to form a continuous superhelix, which is wrapped along its length by histone dimers (Figures 3C and 3D). In the open hypernucleosomes, the "sideway" contacts between histone dimers and the DNA end-to-end stacking are enough to drive the assembly formation, even in the absence of histone stacking interactions as in the closed form.

To exclude a possible influence of the SELEX-based Widom601 DNA sequence on hypernucleosome formation, we next used a native genomic 420-bp DNA sequence (derived from a HeimC3\_31310 gene of LC3 metagenome) for reconstitutions. The EMSA showed typical binding behavior comparable to Widom601 DNA (Figure S2). The number of shifted bands was higher than for the 147-bp Widom DNA due to the greater number of binding sites on the longer native DNA. Importantly, in the high Mg (100 mM) condition, by cryo-EM, we observed formation of hypernucleosomes similar to those formed with Widom601 DNA (Figure S5). The pitch of the native-sequence hypernucleosome was measured to be 25.2 Å, matching that of the closed hypernucleosome formed on Widom601 DNA (25.4 Å).

## The closed and open nucleosomes differ in key interfaces

Three key interfaces are important for nucleosome and hypernucleosome assemblies: (1) histone dimer-DNA interface, (2) histone dimer-dimer interface, and (3) histone dimer stacking interface. Another important contact is the histone-histone interface within the dimer handshake motif, but this is extremely conserved across the phylogenetic tree and is essentially identical between the assemblies (RMSD 0.4 Å over the dimer between  $C\alpha$  atoms).



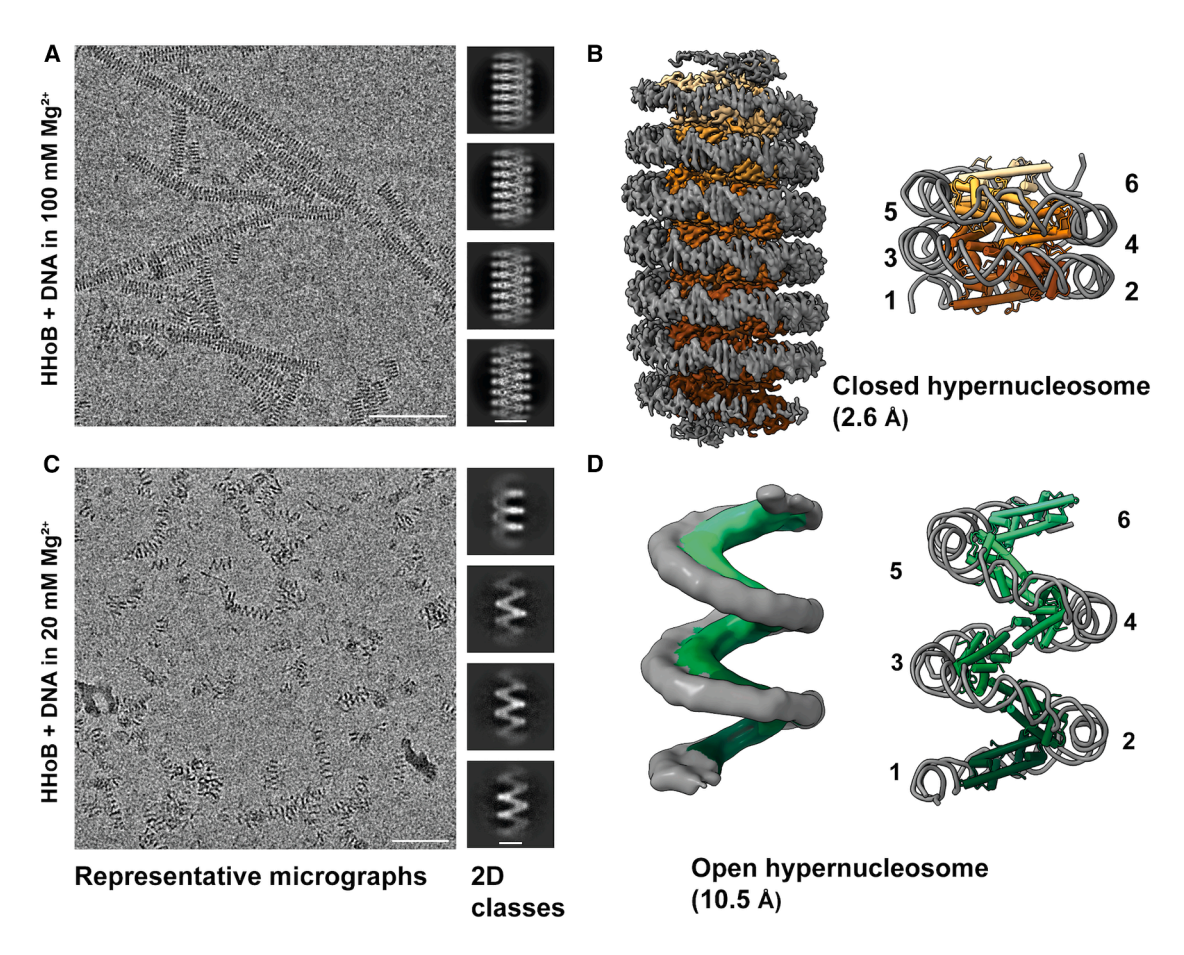


Figure 3. HHoB hypernucleosomes in open and closed states
(A and C) Micrographs (scale bar, 50 nm) and 2D classes (scale bar, 10 nm) of HHoB-DNA at 100 mM (A) and 20 mM (C) MgCl<sub>2</sub>.
(B and D) EM maps and models of closed (B, orange) and open (D, green) hypernucleosomes. Models show 180 bp DNA (gray) and six histone dimers.

The open HHoB hypernucleosome forms a highly extended superhelix without any stacking interactions between histones (Figure 4). This extremely open conformation is fully sustained by the histone-DNA interfaces and minimal histone dimer-dimer interfaces (Figure 4). Each histone dimer in the open state participates in two dimer-dimer contacts (558 + 526 Ų interfaces) and one histone-DNA interface (1,966 Ų area). In the closed hypernucleosome, each histone dimer is involved in two dimer-dimer interfaces (727 + 728 Ų), one histone-DNA interface (1,959 Ų), and two stacking interfaces (1674 + 1676 Ų). Overall, the interface area that a histone dimer participates in within the closed hypernucleosome is  $2.2\times$  larger (6,764/3,050 = 2.2) than in the open conformation, making it much more compact and stable.

The histone-DNA interface is highly conserved and is essentially identical in the open and closed nucleosome states reported here (RMSD 0.4 Å between  $C\alpha$  atoms) (Figure 4). The main residues involved are Arg9, Arg15, Arg21, Lys55, and Lys58 (Figure 1A).

# Histone dimer-dimer interface changes drastically between the open and closed states

Comparison of the histone dimer-dimer interface in the open and closed nucleosome models revealed substantial rearrangement between states, with an RMSD between  $C\alpha$  atoms of a dimer

N+1 of 12.9 Å (if dimers N of the open and closed state are superimposed) (Figure 4A; Video S2). The relative positions of the two neighboring dimers differ strongly in the closed vs. open state. In the closed state, the dimers are positioned at a shallow angle to each other (Figure 4A), allowing for a gentle rise of the helix in a closed hypernucleosome. When we align the dimers N in both closed and open states, and then draw an axis along one of the  $\alpha 2$  helices in each dimer N+1 (chimera X,  $^{41}$  structure analysis tools), it becomes clear that the dimers N and N+1 are positioned at a steeper angle to each other in the open state, compared with the closed state (21° difference, Figure 4A; Video S2); therefore, the rise of the superhelix is also much steeper, allowing for a very open extended structure.

Residues Tyr44, Glu47, Ile48, His51, Arg54, Asp61, and Lys68 are involved in interactions between helices  $\alpha 2$  and  $\alpha 3$  and loop L2 of the interacting histones in the open state (Figures 4B and 4C). In the closed state, residues Leu64 and Gln67 additionally contribute to the dimer-dimer interface, and many of the abovementioned residues change their interaction network. In the open state, the interface area of dimer N with dimer N-1 is 558  $\mathring{A}^2$  compared with 727  $\mathring{A}^2$  in the closed state. Moreover, the His51 and Tyr44 side chains are oriented very differently in the closed and open states (Figures 4B and 4C). Residue



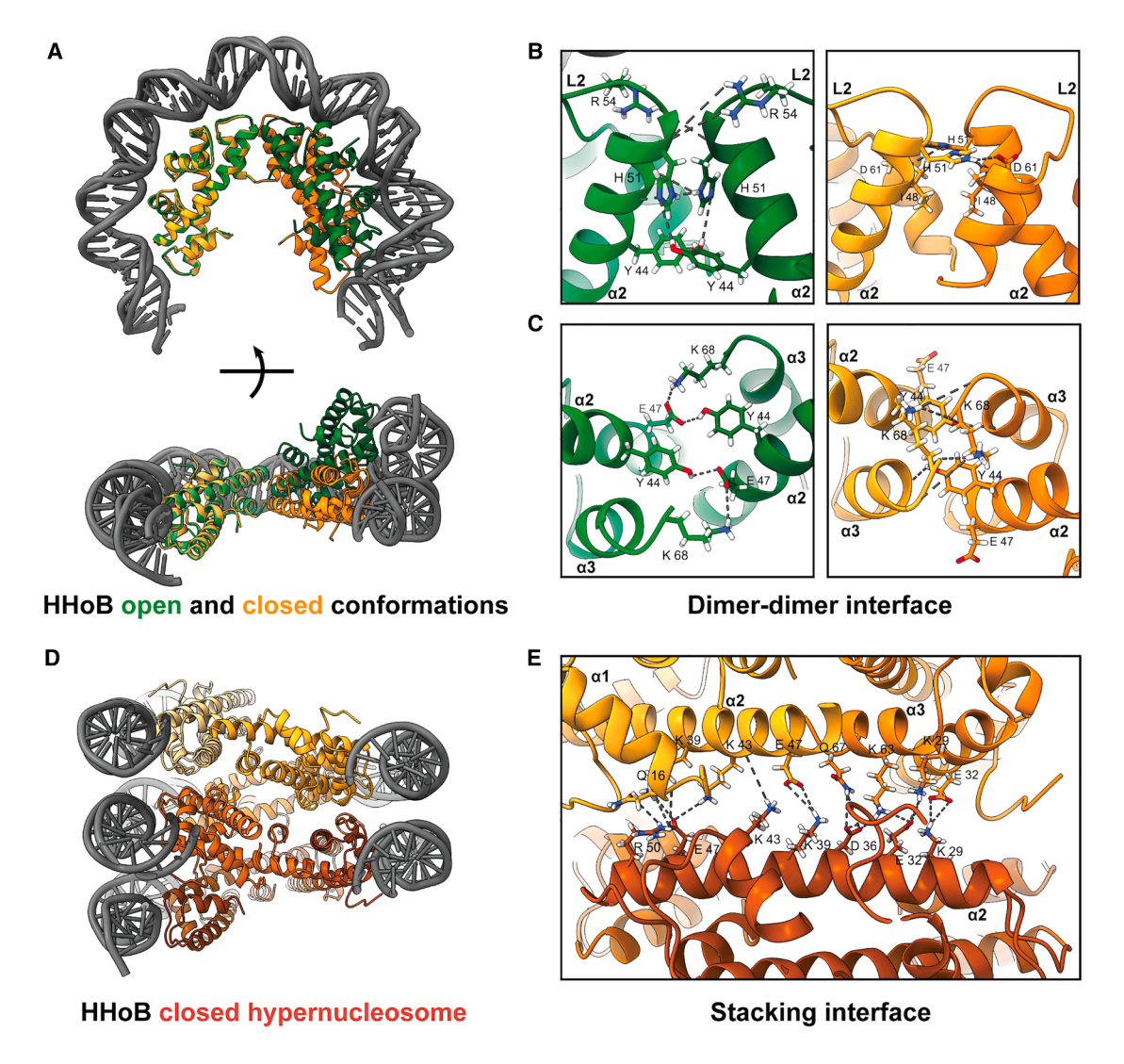


Figure 4. Key interfaces in open (green) and closed (orange) HHoB-DNA

(A) N and N+1 dimers aligned.

(B and C) Dimer-dimer interface key residues: Y44, E47, I48, H51, R54, D61, and K68.

(D) Slice through closed hypernucleosome.

(E) Stacking interface (N, N+2, and N+3 dimers) with key residues Q16, K29, E32, K39, K43, E47, R50, K63, and Q67. Dashed lines: electrostatic/hydrogen bonds.

His51 is highly conserved (with a few exceptions), while others are less conserved. Interactions Tyr44-Glu47, Tyr44-His51, and Glu47-Lys68 are unique to the open state.

Interestingly, the eukaryotic "octasome" formed by four H3-H4 heterodimers also shows an open clam-shell-like conformation. The opening ("pitch") of the octasome open state is  $53~\mbox{\mbox{\sc A}}-\mbox{\sc much}$  closer to the HHoB open state ( $63~\mbox{\sc A}$ ) than to the closed one ( $25~\mbox{\sc A}$ ). Notably, at the central H4-H4 histone interface in the octasome structure, there is also a Tyr residue but at an equivalent of position 48 (HHoB numbering). We hypothesized that if the Tyr helps to stabilize the open state of the HHoB dimer-dimer interface, its exact position on the  $\alpha 2$  helix may define the final degree of nucleosome opening. Therefore, we generated a double mutant ("mut1" Y44A-l48Y) where the original Tyr44 was mutated to

Ala, and instead, a Tyr was introduced at a position 48 to imitate the Tyr position in the H3-H4 octasome. The mutant showed similar DNA binding behavior as the wild-type (WT) HHoB via EMSA (Figure S2). This was expected, as the histone-DNA interface was not affected in the mut1. We then collected a cryo-EM dataset on the mut1 HHoB nucleosomes reconstituted in the 1 mM Mg condition, and we analyzed the data via SPA (Figure S9). In the 2D classes, we observed both closed and open states (Figure 5E), although the nucleosome opening in the open classes was smaller than in the WT HHoB. The 3D reconstruction resulted in a low-resolution map, indicating that the destabilization of the dimer-dimer interface weakens the entire nucleosome or leads to higher conformational heterogeneity. The final EM map shows a decreased nucleosome opening



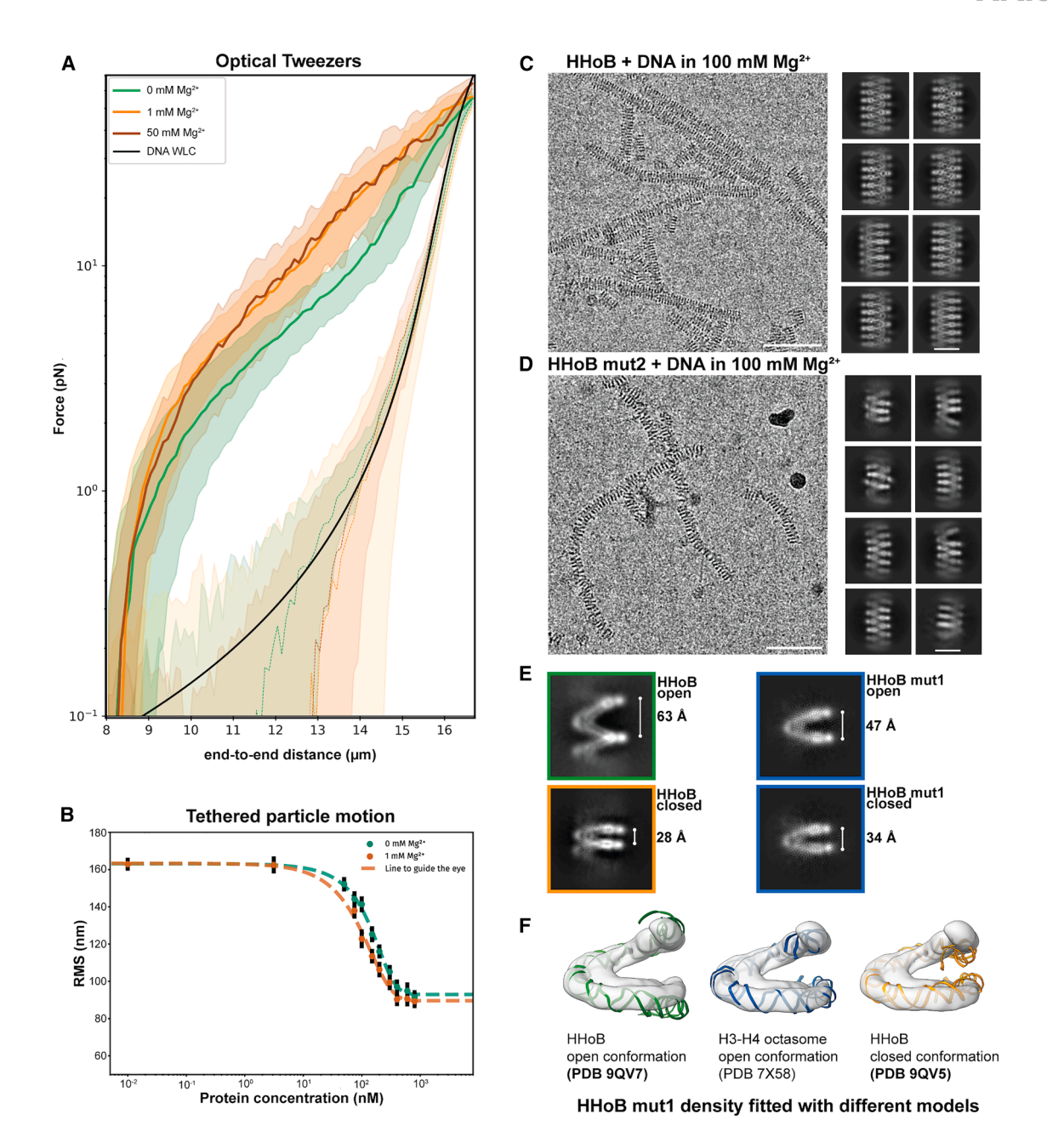


Figure 5. Biophysical analysis of HHoB-DNA complexes

(A) Force-extension curves of HHoB-lambda DNA at 0, 1, and 50 mM MgCl<sub>2</sub> (green, orange, and brown; n = 10). Black line: WLC model.

- (B) TPM of HHoB with 685 bp DNA at varying Mg<sup>2+</sup>; error bars indicate standard deviation.
- (C and D) Micrographs (scale bar, 50 nm) and 2D classes (scale bar, 10 nm) of HHoB-DNA and HHoB mut2-DNA in 100 mM MgCl2.
- (E) 2D classes of HHoB mut1-DNA at 1 mM MgCl<sub>2</sub> (blue) compared with open (green) and closed (orange) WT.
- (F) EM map of HHoB mut1-DNA (gray) fitted with open/closed WT models and H3-H4 octasome (blue).

compared with the WT HHoB open nucleosome (Figures 5F and S9). The degree of nucleosome opening in mut1 open state matched most closely the H3-H4 octasome structure, which has a Tyr in a matching position 48 (Figure S9). This supports our hypothesis regarding the role of Tyr44 in open-state stabilization. Notably, all residues involved in the open HHoB nucleosome dimer-dimer interface are also involved in the closed dimer-dimer

interface; therefore, they cannot be decoupled in a mutagenesis experiment.

# Stacking interface in the closed HHoB hypernucleosome is mediated by electrostatic interactions

Another important contact stabilizing the closed state is the histone stacking interface. Based on the closed hypernucleosome



structure, stacking interactions are primarily mediated by electrostatic interactions between  $\alpha 3$  and  $\alpha 2$  helices of histone dimer N and the  $\alpha 2$  helix of dimer N + 2, and between N  $\alpha 2$  and  $\alpha 1$ , L1 of dimer N + 2. The key residues involved in stacking interactions based on our structure are the following: Gln16, Lys29, Glu32, Asp36, Arg50, and Lys63 (Figure 4E). The exact positions of these residues are not completely conserved between HMfB and most short LC3 histones (Figure 1A), but in both structures, they create a "velcro-like" arrangement of positively and negatively charged residues that mediates the stacking interface.

We generated a triple mutant of the key residues ("mut2" K29A E32A D36A) involved in the stacking interface and tested its ability to form nucleosomes. EMSA showed that the mut2 has similar DNA binding properties to WT (Figure S2), as expected, since the histone-DNA interface remains unaffected by these mutations. We then tested mut2 ability to form hypernucleosomes in a high Mg<sup>2+</sup> condition (100 mM) and examined the samples by cryo-EM (Figure 5E). We observed that the stacking interface mutant can form hypernucleosomes (as not all stacking interactions are disrupted), but they are much less ordered than WT, with a more flexible and "wobbly" appearance (Figures 5D, 5E, and S10). The SPA analysis enriches for more ordered states, and therefore, it does not reflect the whole range of conformations in the mutant nucleosomes. Nonetheless, it reveals a much larger pitch compared with the WT closed hypernucleosomes (Figure S10). This demonstrates that the stacking interface is essential for stabilizing the closed hypernucleosome.

# Biophysical experiments show distinct behavior of HHoB nucleosomes depending on Mg<sup>2</sup> concentration

To investigate the mechanical properties of the HHoB hypernucleosome in response to Mg2+, we performed optical-tweezerbased force-spectroscopy measurements<sup>42,43</sup> using long lambda phage DNA (48,502 bp) as a substrate. The Mg<sup>2+</sup> concentration served as a proxy for chromatin compaction, with cryo-EM data indicating that in the absence of Mg<sup>2+</sup>, the histone-DNA complex exists exclusively in an open conformation. In contrast, samples containing Mg2+ exhibit a mixture of open and closed conformations (1-80 mM Mg<sup>2+</sup>). Force-extension measurements of the HHoB-DNA complex were performed in buffers containing 0, 1, and 50 mM MgCl<sub>2</sub> (Figure 5A). These curves represent the mean ± standard deviation from 10 independent traces. The concentration of HHoB-Atto647N in the protein channel was 200 nM, which is 6.5 times higher than the measured dissociation constant ( $K_D$ ; 30.8 ± 3.7 nM). We overlaid the theoretical worm-like chain (WLC) model for free DNA (Figure 5A), which correlates very well with the free DNA curves from the experiments. The free DNA curves also demonstrate no difference in mechanical properties of DNA in the presence of Mg<sup>2+</sup>. Notably, the overall force-extension curves resemble previously published data on HMfB hypernucleosomes. 14 In the presence of HHoB, the force magnitudes measured for the 0 mM Mg<sup>2+</sup> condition are distinct from those obtained at 1 and 50 mM MgCl<sub>2</sub> (Figure 5A). To quantify these differences, we probed the force difference between histone-DNA complexes and free DNA at low (10  $\mu$ m) and high (13  $\mu$ m) endto-end distances (EED). At low EED, the measured force differences were 2.01  $\pm$  0.36 pN for 0 mM, 3.52  $\pm$  0.59 pN for 1 mM, and 3.27  $\pm$  0.68 pN for 50 mM MgCl<sub>2</sub> (N = 10). While at high EED, the force differences were  $6.63 \pm 0.56$  pN for 0 mM,  $12.73 \pm 2.03$  pN for 1 mM, and  $13.41 \pm 1.94$  pN for 50 mM MgCl<sub>2</sub> (N=10). Paired t tests confirmed that the differences between 0 mM and both 1 and 50 mM MgCl<sub>2</sub> were statistically significant at both EEDs (p < 0.01). It is worth noting that owing to clogging issues in the microfluidic flow channels at higher protein concentrations, our experiments are limited in probing the full saturation regime of histone binding to DNA. However, clearly, the consistent and significant force differences across conditions suggest a genuine Mg<sup>2+</sup>-dependent modulation of DNA compaction by HHoB, possibly arising from hypernucleosome stacking interactions, cooperative histone binding, or a combination of both.

To further investigate the structural changes induced by HHoB upon DNA binding in solution, we conducted tethered particle motion (TPM) experiments using a linear 685-bp DNA fragment. TPM allows us to probe a full range of protein concentrations up to the full saturation regime. In TPM, a bead is tethered to a glass surface by a DNA molecule. 44 DNA compaction can be quantified by measuring the decrease in root-mean-squared displacement (RMSd) of the bead relative to the glass surface. 14,45 Individual data points represent the average of N > 100 protein-DNA complexes. Titration of HHoB induced a gradual decrease in RMSd, confirming that HHoB wraps and compacts the DNA (Figure 5C). Next, we examined the effect of  $\mathrm{Mg}^{2+}$  in a protein titration experiment, which showed that in the presence of Mg<sup>2+</sup>, hypernucleosome formation shifts toward lower protein concentrations, and the RMSd of the hypernucleosome structure obtained at protein saturation was more compact than in its absence (Figure 5C). To compare the differences quantitatively, we measured the RMSd at the "midpoint concentration" (150 nM HHoB), where the RMSd lies in between the unbound and saturated states. We also compared the RMSd at the fully saturated state (800 nM HHoB). At the midpoint concentration, the RMSd values were 125.3  $\pm$  3.2 nm at 0 mM Mg<sup>2+</sup> and 113.5  $\pm$  2.8 nm at 1 mM Mg<sup>2+</sup>. At saturation, the RMSd values were 91.5 ± 2.7 nm at 0 mM  $Mg^{2+}$  and 89.3 ± 2.6 nm at 1 mM  $Mg^{2+}$ . Unpaired t tests confirmed statistically significant differences at both midpoint and saturating concentrations (p < 0.01). We note that when the DNA template is longer (685 bp in TPM experiments), the hypernucleosomes will also be able to form at lower Mg concentrations, while stacking of individual nucleosomes needs higher Mg concentrations (in our cryo-EM experiments). These biophysical experiments provide direct evidence that Mg2+ modulates hypernucleosome mechanical properties to form a more compacted state, as higher forces are needed to disrupt the chromatin fiber in the presence of Mg2+, rather than in its absence, and is in perfect agreement with our cryo-EM observations.

#### **DISCUSSION**

#### Closed nucleosome state is conserved across archaea

This study provides the first structural insights into Asgard chromatin, expanding our understanding beyond the better-studied Euryarchaeota. 7,15,46,47 Asgard archaea, and Hodarchaea in particular, 18 are the closest living archaeal relatives to eukaryotes known to date, which makes studying their genome organization extremely important in the context of evolution. Here, we characterized the tail-less histone HHoB from LC3 Asgard Hodarchaea



and demonstrated that it forms nucleosomes in two distinct conformations—closed and open.

All previously reported archaeal nucleosome structures were in a closed conformation (Figure S11). <sup>7,15</sup> This includes the classical closed nucleosomes formed by Euryarchaeal HMfB<sup>7</sup> and HTkA, <sup>15</sup> as well as the "slinky" arrangement of HTkA. <sup>15</sup> Histone dimer-dimer and stacking interfaces in the slinky <sup>15</sup> and classical <sup>7</sup> Euryarchaeal nucleosome structures are consistent with the HHoB closed state. Since both HMfB/HTkA and HHoB histones can form closed nucleosomes, this closed conformation appears to be conserved across distant archaeal groups, such as Asgard and Euryarchaeota. Our findings also experimentally validate the earlier prediction <sup>9</sup> that HHoB LC3 can form closed hypernucleosomes, engaging interactions at the stacking interface. Notably, the open Asgard HHoB nucleosome conformation is novel and was not predicted in previous studies.

#### Open hypernucleosomes as an Asgard innovation

The HHoB open state reported here represents a distinct structural configuration of archaeal chromatin. The HHoB open state has a different dimer-dimer interface, compared with that of the closed state (and to all structures reported previously<sup>7,15</sup>), and is characterized by a complete absence of histone stacking.

Our open HHoB nucleosome structure is characterized by key interactions between Tyr44-Glu47 and Tyr44-His51. All three amino acids are conserved in four out of ten LC3 histones-HHoB, HHoJ, HHoE, and HHoH. Notably, the key residue Tyr44 occurs in 11.5% of Asgard histones, based on recent datasets. 16,48 Tyr44 appears substantially enriched (44.7%) within a subset of Asgard lineages including Hodarchaea (Figure S12B). When we consider histones in all archaeal groups, the frequency of Tyr44 drops to 3.5%. In all annotated Euryarchaeal histones, Tyr44 is only there in 0.1% cases (1 sequence out of 917 analyzed) (Figure S12). This suggests that the open nucleosome state could be a unique innovation of Asgard archaea and may be relatively widespread among them, while the open state should be mostly absent in Euryarchaea. Importantly, a eukaryotic nucleosome assembly "H3-H4" octasome displays an open state as well. 12 It was suggested that the H3-H4 assembly might be ancestral<sup>49</sup> to the canonical nucleosomes. In that light, it is striking, that the Asgard open nucleosome resembles the conformation of the potentially ancestral eukaryotic H3-H4 assembly, indicating the open conformation as an intermediate step in nucleosome evolution (see comparison in Figure S11). However, more experimental evidence of open nucleosome examples is needed to more clearly define the sequence features responsible for this conformation. Notably, AlphaFold3<sup>50</sup> is unable to predict open structures even for the HHoB histone, potentially due to training bias, but instead predicts a closed conformation for all.

We speculate that the open nucleosome state may confer particular advantages for Asgard archaea, especially in enabling faster and more efficient histone exchange, compared with the highly compact closed assembly. Asgards often encode a larger number of "nucleosomal" histone variants, 48 compared with Euryarchaea, which typically encode only one or two (HMfA/B, HTkA/B). 16,51 To exchange a histone dimer even at the end of

a closed hypernucleosome, numerous interfaces must be disrupted (stacking, dimer-dimer, dimer-DNA), whereas in the open assembly, the stacking interface is absent, making histone exchange less energetically costly. Additionally, the open chromatin state may minimize steric clashes involving histones with extended structural elements, such as N- or C-terminal  $\alpha$  helices or tails-features more frequently observed in Asgard histones compared with Euryarchaea-thus facilitating the "evolutionary exploration" of histone extensions in Asgard archaea. We also note a high variability of histone fold sequence among Asgard histones (26.7% mean sequence identity; Figure S12), potentially indicating high variability of conditions that chromatin needs to adapt to in different archaea, which is strikingly different to an extremely high sequence conservation of histone fold in eukaryotes<sup>10,16</sup> (99.1% mean identity; Figure S12). This is in line with a proposal from a recent study, 16 that Asgards have not yet "settled" on a certain set of histones, as did the last common eukaryotic ancestor.

The presence of open Asgard hypernucleosomes also suggests a stable yet dynamic chromatin structure, where DNA is bound by histones but both remain accessible for chromatin modification factors-potential "readers" and "writers" predicted in Asgard archaea.<sup>52</sup> The open state also could be easier for the DNA machinery to passage through than the closed state, based on the lower number of contacts that needs to be broken. In contrast, closed hypernucleosomes may limit the accessibility of histones and DNA more than the open hypernucleosomes, suggesting a regulatory interplay of the two states. This balance of stability and accessibility could be particularly beneficial for thermophilic and hyperthermophilic Asgard species, which must stabilize their DNA under extreme conditions via histone association while maintaining accessibility.<sup>53</sup> Interestingly, the last common ancestor of Asgard archaea is suggested to have been a thermophile.<sup>54</sup>

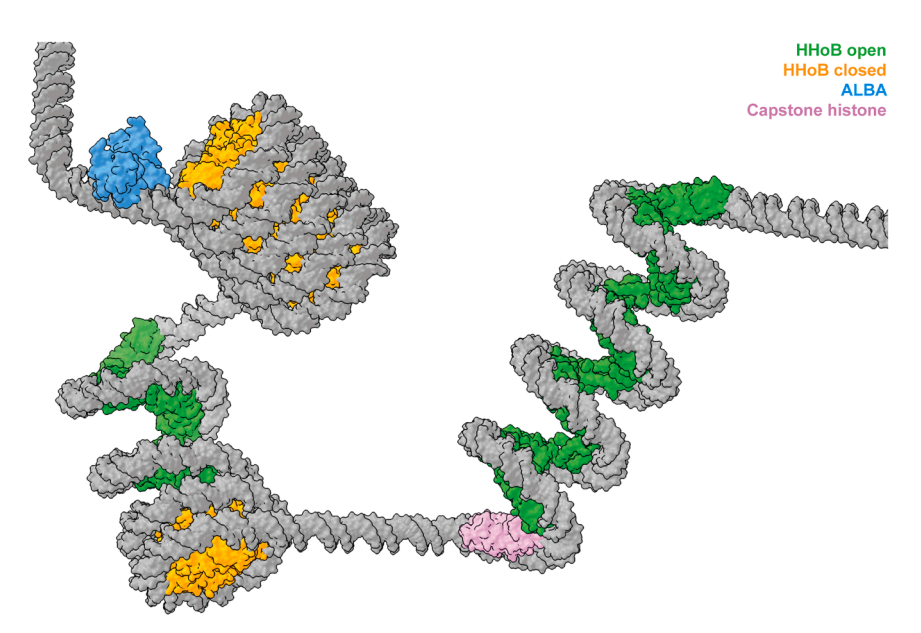
# Mechanisms of Mg<sup>2+</sup>-based nucleosome-state regulation

We investigated the effect of Mg<sup>2+</sup> concentrations on chromatin structure, as Mg<sup>2+</sup> plays a crucial role in nucleosome-state regulation in archaea and eukaryotes. We found that within a wide range of Mg<sup>2+</sup> concentrations (1–60 mM), Asgard histone HHoB forms both closed and open assemblies. At higher Mg<sup>2+</sup> concentrations, HHoB leads to the formation of long closed hypernucleosomes.

Our results suggest a possible mechanism for Mg<sup>2+</sup>-dependent regulation of archaeal chromatin structure. Many archaea use a "salt-in" mechanism<sup>55</sup> to adjust intracellular ion concentrations based on extracellular levels. In this context, Mg<sup>2+</sup> could regulate chromatin state by binding to the negatively charged DNA phosphate backbone, thus shielding charges. At higher Mg<sup>2+</sup> concentrations, DNA gyres in hypernucleosomes may move closer together, promoting a closed state that stabilizes protein-protein interactions at both the histone dimer-dimer and stacking interfaces. We further demonstrated through EMSA that the cooperativity of HHoB-DNA binding is generally much lower, compared with Euryarchaeal HMfB, in "zero Mg<sup>2+</sup>" conditions. Notably, the cooperativity of HHoB binding increases with higher Mg<sup>2+</sup> concentrations, correlating with

### **Article**





increased formation of closed hypernucleosomes. This suggests that Mg<sup>2+</sup> may play a role in regulating chromatin states through its effect on histone-DNA binding cooperativity. Our results suggest that the cooperativity of HHoB binding to the DNA is defined by the synergy of three factors: Mg shielding DNA charges, formation of dimer-dimer, and stacking interfaces.

#### **Asgard chromatin model**

The current model of archaeal chromatin may be described as "variable beads on a string," where in each nucleosome, a variable number (N) of histone dimers associates with DNA, wrapping it into hypernucleosomes of 30  $\times$  N bp length. Our work suggests that this model can now also be applied to describe Asgard chromatin. We observed the formation of long, stable hypernucleosomes in both closed and open states, formed by just one histone variant out of ten encoded in the genome. Taking into account the presence of nine other types of histones in the LC3 metagenome, we expect both closed and open hypernucleosomes of variable length to be formed locally by one or several types of histones (Figure 6). Meanwhile, other types of histones (with lower propensity to form hypernucleosomes) as well as nucleoid-associated proteins could act as capstones<sup>56</sup> and roadblocks, respectively, thus regulating the size and spread of hypernucleosomes and DNA accessibility. The prevalence of open vs. closed conformations could be regulated either by Mg<sup>2+</sup> concentration or by other local environment factors (cations, polycations) or could be stabilized by additional protein players. Overall, further extensive structural and functional studies are required to understand the full conformational landscape of Asgard chromatin to shed light on the role of multiple histone variants, including histones with tails, and how they can shape and regulate chromatin organization.

#### **Limitations of the study**

Our study demonstrates that  $Mg^{2+}$  ions (as well as  $Zn^{2+}$  and  $Ca^{2+}$ ) influence the structural state of Asgard chromatin. However,

#### Figure 6. Asgard variable beads-on-astring chromatin model

Hypernucleosomes of varying lengths either in open (green) or closed (yellow) conformations. Other histone variants (pink) and nucleoid-associated proteins like Alba (blue) could act as capstones and roadblocks.

given the current lack of information about intracellular ion concentrations in Asgard archaea, we cannot exclude the possibility that other positively charged molecules may exert similar effects *in vivo* instead of or together with Mg<sup>2+</sup>.

In the cryo-EM analysis of *in-vitro*-reconstituted chromatin, we observed extended hypernucleosomes reaching  ${\sim}0.5~\mu m$  in length under 100 mM  ${\rm Mg}^{2+}$  conditions. This corresponds to  ${\sim}200$  superhelical turns, encompassing up to  ${\sim}15~kbp$  DNA. However,

the physiological length of such assemblies in cells remains to be determined by other approaches.

#### **RESOURCE AVAILABILITY**

#### Lead contact

Correspondence and requests for materials should be addressed to Svetlana O. Dodonova (svetlana.dodonova@embl.de).

#### **Materials availability**

Materials are available from Svetlana O. Dodonova upon request under a material transfer agreement.

#### **Data and code availability**

- The cryo-EM maps and model coordinates were deposited with the Electron Microscopy Database (EMDB) and Protein Data Bank (PDB) under accession codes EMD-53386 and PDB: 9QV5 (closed nucleosome in 1 mM Mg<sup>2+</sup>), EMD-53388 and PDB: 9QV7 (open nucleosome in 1 mM Mg<sup>2+</sup>), EMD-53390 (open nucleosome in 0 Mg<sup>2+</sup>), EMD-53387 and PDB: 9QV6 (closed hypernucleosome), and EMD-53389 (open hypernucleosome).
- This paper does not report original code.
- Any additional information required to reanalyze the data reported in this
  paper is available from the lead contact upon request.

#### **ACKNOWLEDGMENTS**

This work is supported by the European Union (ERC Starting Grant 3DchromArchaea, grant agreement no. 101076671, to S.O.D.). H.M.R. acknowledges support by the EMBL PhD program. R.T.D. was supported by the Dutch Research Council (OCENW.GROOT.2019.01). We thank Wim Hagen, Felix Weiss, Joseph Bartho, and Sebastian Unger for technical assistance; Alexander Marchanka for help with mutagenesis and initial optimization; EMBL PEP core facility and Karine Lapouge for support with protein quality control experiments; and Christoph Müller and Fredrika Rajer for helpful comments on the manuscript.

Funded by the European Union, the views and opinions expressed are, however, those of the authors only and do not necessarily reflect those of the European Union or the European Research Council Executive Agency. Neither the European Union nor the granting authority can be held responsible for them.



# **Molecular Cell**

#### **AUTHOR CONTRIBUTIONS**

H.M.R. prepared the DNA and protein constructs, purified the proteins and DNA, performed in vitro reconstitutions, performed EMSA experiments, prepared cryo-EM grids, collected and processed cryo-EM data, and built models. H.M.R. and N.L.-B. performed the force-extension experiments. M.K.C. carried out the footprinting EMSA and TPM experiments under supervision of R.T.D. With help from T.Q., H.M.R. analyzed force-extension data. S.O.D. conceived the study, supervised the research, and wrote the manuscript with input from all authors.

#### **DECLARATION OF INTERESTS**

The authors declare no competing interests.

#### **STAR**\*METHODS

Detailed methods are provided in the online version of this paper and include the following:

- KEY RESOURCES TABLE
- EXPERIMENTAL MODEL AND STUDY PARTICIPANT DETAILS
  - o Plasmids and strains
- METHOD DETAILS
  - o HHoB mutagenesis
  - Protein expression and purification
  - o DNA sequences and preparation
  - o In-vitro reconstitution and binding affinity measurements
  - Sample preparation for crvo-EM
  - o Data collection
  - o Data processing and analysis
  - o Model fitting and refinement
  - o Protein labelling with fluorescent dye
  - o Force Spectroscopy measurement and analysis
  - o Tethered Particle Motion
  - o Multi-Sequence Alignment
- QUANTIFICATION AND STATISTICAL ANALYSIS

#### SUPPLEMENTAL INFORMATION

Supplemental information can be found online at https://doi.org/10.1016/j. molcel.2025.10.001.

Received: April 17, 2025 Revised: August 19, 2025 Accepted: October 1, 2025

#### **REFERENCES**

- 1. Luger, K., Mäder, A.W., Richmond, R.K., Sargent, D.F., and Richmond, T.J. (1997). Crystal structure of the nucleosome core particle at 2.8 A resolution. Nature 389, 251-260. https://doi.org/10.1038/38444.
- 2. Starich, M.R., Sandman, K., Reeve, J.N., and Summers, M.F. (1996). NMR structure of HMfB from the hyperthermophile. Methanothermus fervidus. confirms that this archaeal protein is a histone. J. Mol. Biol. 255, 187-203. https://doi.org/10.1006/jmbi.1996.0016.
- 3. Decanniere, K., Babu, A.M., Sandman, K., Reeve, J.N., and Heinemann, U. (2000). Crystal structures of recombinant histones HMfA and HMfB from the hyperthermophilic archaeon Methanothermus fervidus, J. Mol. Biol. 303, 35-47. https://doi.org/10.1006/jmbi.2000.4104.
- 4. Sandman, K., and Reeve, J.N. (2006). Archaeal histones and the origin of the histone fold. Curr. Opin. Microbiol. 9, 520-525. https://doi.org/10. 1016/j.mib.2006.08.003.
- 5. Arents, G., Burlingame, R.W., Wang, B.C., Love, W.E., and Moudrianakis, E.N. (1991). The nucleosomal core histone octamer at 3.1 A resolution:

- a tripartite protein assembly and a left-handed superhelix. Proc. Natl. Acad. Sci. USA 88, 10148-10152. https://doi.org/10.1073/pnas.88.
- 6. Sandman, K., Grayling, R.A., Dobrinski, B., Lurz, R., and Reeve, J.N. (1994). Growth-phase-dependent synthesis of histones in the archaeon Methanothermus fervidus. Proc. Natl. Acad. Sci. USA 91, 12624-12628. https://doi.org/10.1073/pnas.91.26.12624.
- 7. Mattiroli, F., Bhattacharyya, S., Dyer, P.N., White, A.E., Sandman, K., Burkhart, B.W., Byrne, K.R., Lee, T., Ahn, N.G., Santangelo, T.J., et al. (2017). Structure of histone-based chromatin in Archaea. Science 357. 609-612. https://doi.org/10.1126/science.aaj1849.
- 8. Maruyama, H., Harwood, J.C., Moore, K.M., Paszkiewicz, K., Durley, S.C., Fukushima, H., Atomi, H., Takeyasu, K., and Kent, N.A. (2013). An alternative beads-on-a-string chromatin architecture in Thermococcus kodakarensis. EMBO Rep. 14, 711-717. https://doi.org/10.1038/embor.2013.94.
- 9. Henneman, B., van Emmerik, C., van Ingen, H., and Dame, R.T. (2018). Structure and function of archaeal histones. PLoS Genet. 14, e1007582. https://doi.org/10.1371/journal.pgen.1007582.
- 10. Phillips, E.O.N., and Gunjan, A. (2022). Histone variants: The unsung guardians of the genome. DNA Repair (Amst) 112, 103301. https://doi. org/10.1016/j.dnarep.2022.103301.
- 11. Hatazawa, S., Horikoshi, N., and Kurumizaka, H. (2025). Structural diversity of noncanonical nucleosomes: Functions in chromatin. Curr. Opin. Struct. Biol. 92, 103054. https://doi.org/10.1016/j.sbi.2025.103054.
- 12. Nozawa, K., Takizawa, Y., Pierrakeas, L., Sogawa-Fujiwara, C., Saikusa, K., Akashi, S., Luk, E., and Kurumizaka, H. (2022). Cryo-electron microscopy structure of the H3-H4 octasome: A nucleosome-like particle without histones H2A and H2B. Proc. Natl. Acad. Sci. USA 119, e2206542119. https://doi.org/10.1073/pnas.2206542119.
- 13. Zhou, K., Gaullier, G., and Luger, K. (2019). Nucleosome structure and dynamics are coming of age. Nat. Struct. Mol. Biol. 26, 3-13. https://doi.org/ 10.1038/s41594-018-0166-x.
- 14. Henneman, B., Brouwer, T.B., Erkelens, A.M., Kuijntjes, G.J., van Emmerik, C., van der Valk, R.A., Timmer, M., Kirolos, N.C.S., van Ingen, H., van Noort, J., and Dame, R.T. (2021). Mechanical and structural properties of archaeal hypernucleosomes. Nucleic Acids Res. 49, 4338-4349. https://doi.org/10.1093/nar/gkaa1196.
- 15. Bowerman, S., Wereszczynski, J., and Luger, K. (2021). Archaeal chromatin 'slinkies' are inherently dynamic complexes with deflected DNA wrapping pathways. Elife 10, e65587. https://doi.org/10.7554/ eLife.65587.
- 16. Hocher, A., and Warnecke, T. (2024). Nucleosomes at the Dawn of Eukaryotes. Genome Biol. Evol. 16, evae029. https://doi.org/10.1093/ gbe/evae029.
- 17. Zaremba-Niedzwiedzka, K., Caceres, E.F., Saw, J.H., Bäckström, D., Juzokaite, L., Vancaester, E., Seitz, K.W., Anantharaman, K., Starnawski, P., Kjeldsen, K.U., et al. (2017). Asgard archaea illuminate the origin of eukaryotic cellular complexity. Nature 541, 353-358. https://doi.org/10.1038/nature21031.
- 18. Eme, L., Tamarit, D., Caceres, E.F., Stairs, C.W., De Anda, V., Schön, M.E., Seitz, K.W., Dombrowski, N., Lewis, W.H., Homa, F., et al. (2023). Inference and reconstruction of the heimdallarchaeial ancestry of eukaryotes. Nature 618, 992-999. https://doi.org/10.1038/s41586-023-06186-2.
- 19. Vosseberg, J., van Hooff, J.J.E., Köstlbacher, S., Panagiotou, K., Tamarit, D., and Ettema, T.J.G. (2024). The emerging view on the origin and early evolution of eukaryotic cells. Nature 633, 295-305. https://doi.org/10. 1038/s41586-024-07677-6.
- 20. Irwin, N.A.T., and Richards, T.A. (2024). Self-assembling viral histones are evolutionary intermediates between archaeal and eukaryotic nucleosomes. Nat. Microbiol. 9, 1713-1724. https://doi.org/10.1038/s41564-024-01707-9
- 21. Valencia-Sánchez, M.I., Abini-Agbomson, S., Wang, M., Lee, R., Vasilyev, N., Zhang, J., De Ioannes, P., La Scola, B., Talbert, P., Henikoff, S., et al.

#### **Article**



- (2021). The structure of a virus-encoded nucleosome. Nat. Struct. Mol. Biol. 28, 413–417. https://doi.org/10.1038/s41594-021-00585-7.
- Lowary, P.T., and Widom, J. (1998). New DNA sequence rules for high affinity binding to histone octamer and sequence-directed nucleosome positioning. J. Mol. Biol. 276, 19–42. https://doi.org/10.1006/jmbi.1997.1494.
- Dodonova, S.O., Zhu, F., Dienemann, C., Taipale, J., and Cramer, P. (2020). Nucleosome-bound SOX2 and SOX11 structures elucidate pioneer factor function. Nature 580, 669–672. https://doi.org/10.1038/s41586-020-2195-y.
- Bilokapic, S., Strauss, M., and Halic, M. (2018). Histone octamer rearranges to adapt to DNA unwrapping. Nat. Struct. Mol. Biol. 25, 101–108. https://doi.org/10.1038/s41594-017-0005-5.
- Bailey, K.A., Chow, C.S., and Reeve, J.N. (1999). Histone stoichiometry and DNA circularization in archaeal nucleosomes. Nucleic Acids Res. 27, 532–536. https://doi.org/10.1093/nar/27.2.532.
- Romani, A. (2007). Regulation of magnesium homeostasis and transport in mammalian cells. Arch. Biochem. Biophys. 458, 90–102. https://doi. org/10.1016/j.abb.2006.07.012.
- Romani, A., and Scarpa, A. (1992). Regulation of cell magnesium. Arch. Biochem. Biophys. 298, 1–12. https://doi.org/10.1016/0003-9861(92) 90086-c.
- Nagata, M., Ishino, S., Yamagami, T., Ogino, H., Simons, J.R., Kanai, T., Atomi, H., and Ishino, Y. (2017). The Cdc45/RecJ-like protein forms a complex with GINS and MCM, and is important for DNA replication in Thermococcus kodakarensis. Nucleic Acids Res. 45, 10693–10705. https://doi.org/10.1093/nar/gkx740.
- van der Valk, R.A., Vreede, J., Qin, L., Moolenaar, G.F., Hofmann, A., Goosen, N., and Dame, R.T. (2017). Mechanism of environmentally driven conformational changes that modulate H-NS DNA-bridging activity. Elife 6, e27369. https://doi.org/10.7554/eLife.27369.
- Rashid, F.M., Crémazy, F.G.E., Hofmann, A., Forrest, D., Grainger, D.C., Heermann, D.W., and Dame, R.T. (2023). The environmentally-regulated interplay between local three-dimensional chromatin organisation and transcription of proVWX in E. coli. Nat. Commun. 14, 7478. https://doi. org/10.1038/s41467-023-43322-y.
- Imachi, H., Nobu, M.K., Nakahara, N., Morono, Y., Ogawara, M., Takaki, Y., Takano, Y., Uematsu, K., Ikuta, T., Ito, M., et al. (2020). Isolation of an archaeon at the prokaryote-eukaryote interface. Nature 577, 519–525. https://doi.org/10.1038/s41586-019-1916-6.
- Rodrigues-Oliveira, T., Wollweber, F., Ponce-Toledo, R.I., Xu, J., Rittmann, S.K.R., Klingl, A., Pilhofer, M., and Schleper, C. (2023). Actin cytoskeleton and complex cell architecture in an Asgard archaeon. Nature 613, 332–339. https://doi.org/10.1038/s41586-022-05550-y.
- Punjani, A., Rubinstein, J.L., Fleet, D.J., and Brubaker, M.A. (2017). cryoSPARC: algorithms for rapid unsupervised cryo-EM structure determination. Nat. Methods 14, 290–296. https://doi.org/10.1038/ nmeth.4169.
- Adams, P.D., Afonine, P.V., Bunkóczi, G., Chen, V.B., Davis, I.W., Echols, N., Headd, J.J., Hung, L.W., Kapral, G.J., Grosse-Kunstleve, R.W., et al. (2010). PHENIX: a comprehensive Python-based system for macromolecular structure solution. Acta Crystallogr. D Biol. Crystallogr. 66, 213–221. https://doi.org/10.1107/S0907444909052925.
- Emsley, P., and Cowtan, K. (2004). Coot: model-building tools for molecular graphics. Acta Crystallogr. D Biol. Crystallogr. 60, 2126–2132. https:// doi.org/10.1107/S0907444904019158.
- Croll, T.I. (2018). ISOLDE: a physically realistic environment for model building into low-resolution electron-density maps. Acta Crystallogr. D Struct. Biol. 74, 519–530. https://doi.org/10.1107/S2059798318002425.
- Visvanathan, A., Ahmed, K., Even-Faitelson, L., Lleres, D., Bazett-Jones, D.P., and Lamond, A.I. (2013). Modulation of Higher Order Chromatin Conformation in Mammalian Cell Nuclei Can Be Mediated by Polyamines and Divalent Cations. PLoS One 8, e67689. https://doi.org/ 10.1371/journal.pone.0067689.

- Ohyama, T. (2019). New Aspects of Magnesium Function: A Key Regulator in Nucleosome Self-Assembly, Chromatin Folding and Phase Separation. Int. J. Mol. Sci. 20, 4232. https://doi.org/10.3390/ijms20174232.
- Bepler, T., Morin, A., Rapp, M., Brasch, J., Shapiro, L., Noble, A.J., and Berger, B. (2019). Positive-unlabeled convolutional neural networks for particle picking in cryo-electron micrographs. Nat. Methods 16, 1153– 1160. https://doi.org/10.1038/s41592-019-0575-8.
- Maguire, M.E., and Cowan, J.A. (2002). Magnesium chemistry and biochemistry. Biometals 15, 203–210. https://doi.org/10.1023/a:1016058229972.
- Meng, E.C., Goddard, T.D., Pettersen, E.F., Couch, G.S., Pearson, Z.J., Morris, J.H., and Ferrin, T.E. (2023). UCSF ChimeraX: Tools for structure building and analysis. Protein Sci. 32, e4792. https://doi.org/10.1002/ pro.4792.
- Bustamante, C.J., Chemla, Y.R., Liu, S., and Wang, M.D. (2021). Optical tweezers in single-molecule biophysics. Nat. Rev. Methods Primers 1, 25. https://doi.org/10.1038/s43586-021-00021-6.
- Renger, R., Morin, J.A., Lemaitre, R., Ruer-Gruss, M., Jülicher, F., Hermann, A., and Grill, S.W. (2022). Co-condensation of proteins with single- and double-stranded DNA. Proc. Natl. Acad. Sci. USA 119, e2107871119. https://doi.org/10.1073/pnas.2107871119.
- Henneman, B., Erkelens, A.M., Heinsman, J., Battjes, J., and Dame, R.T. (2024). Quantitation of DNA Binding Affinity Using Tethered Particle Motion. Methods Mol. Biol. 2819, 497–518. https://doi.org/10.1007/978-1-0716-3930-6\_23.
- van der Valk, R.A., Laurens, N., and Dame, R.T. (2017). Tethered Particle Motion Analysis of the DNA Binding Properties of Architectural Proteins. Methods Mol. Biol. 1624, 127–143. https://doi.org/10.1007/978-1-4939-7098-8
- Nalabothula, N., Xi, L., Bhattacharyya, S., Widom, J., Wang, J.P., Reeve, J.N., Santangelo, T.J., and Fondufe-Mittendorf, Y.N. (2013). Archaeal nucleosome positioning in vivo and in vitro is directed by primary sequence motifs. BMC Genomics 14, 391. https://doi.org/10.1186/ 1471-2164-14-391.
- Rojec, M., Hocher, A., Stevens, K.M., Merkenschlager, M., and Warnecke, T. (2019). Chromatinization of Escherichia coli with archaeal histones. Elife 8, e49038. https://doi.org/10.7554/eLife.49038.
- Schwab, S., Hu, Y., van Erp, B., Cajili, M.K.M., Hartmann, M.D., Hernandez Alvarez, B., Alva, V., Boyle, A.L., and Dame, R.T. (2024). Histones and histone variant families in prokaryotes. Nat. Commun. 15, 7950. https://doi.org/10.1038/s41467-024-52337-y.
- Malik, H.S., and Henikoff, S. (2003). Phylogenomics of the nucleosome.
   Nat. Struct. Biol. 10, 882–891. https://doi.org/10.1038/nsb996.
- Abramson, J., Adler, J., Dunger, J., Evans, R., Green, T., Pritzel, A., Ronneberger, O., Willmore, L., Ballard, A.J., Bambrick, J., et al. (2024). Accurate structure prediction of biomolecular interactions with AlphaFold 3. Nature 630, 493–500. https://doi.org/10.1038/s41586-024-07487-w.
- Stevens, K.M., Hocher, A., and Warnecke, T. (2022). Deep Conservation of Histone Variants in Thermococcales Archaea. Genome Biol. Evol. 14, evab274. https://doi.org/10.1093/gbe/evab274.
- 52. Grau-Bové, X., Navarrete, C., Chiva, C., Pribasnig, T., Antó, M., Torruella, G., Galindo, L.J., Lang, B.F., Moreira, D., López-Garcia, P., et al. (2022). A phylogenetic and proteomic reconstruction of eukaryotic chromatin evolution. Nat. Ecol. Evol. 6, 1007–1023. https://doi.org/10.1038/s41559-022-01771-6.
- Hocher, A., Borrel, G., Fadhlaoui, K., Brugère, J.-F., Gribaldo, S., and Warnecke, T. (2021). Growth temperature is the principal driver of chromatinization in archaea. Preprint at bioRxiv. https://doi.org/10.1101/2021.07. 08.451601.
- Lu, Z., Xia, R., Zhang, S., Pan, J., Liu, Y., Wolf, Y.I., Koonin, E.V., and Li, M. (2024). Evolution of optimal growth temperature in Asgard archaea inferred from the temperature dependence of GDP binding to EF-1A. Nat. Commun. 15, 515. https://doi.org/10.1038/s41467-024-44806-1.



### Molecular Cell Article

- Oren, A. (2008). Microbial life at high salt concentrations: phylogenetic and metabolic diversity. Saline Syst. 4, 2. https://doi.org/10.1186/1746-1448-4-2.
- Stevens, K.M., Swadling, J.B., Hocher, A., Bang, C., Gribaldo, S., Schmitz, R.A., and Warnecke, T. (2020). Histone variants in archaea and the evolution of combinatorial chromatin complexity. Proc. Natl. Acad. Sci. USA 117, 33384–33395. https://doi.org/10.1073/pnas.2007056117.
- Mastronarde, D.N. (2005). Automated electron microscope tomography using robust prediction of specimen movements. J. Struct. Biol. 152, 36–51. https://doi.org/10.1016/j.jsb.2005.07.007.
- Goddard, T.D., Huang, C.C., Meng, E.C., Pettersen, E.F., Couch, G.S., Morris, J.H., and Ferrin, T.E. (2018). UCSF ChimeraX: Meeting modern challenges in visualization and analysis. Protein Sci. 27, 14–25. https:// doi.org/10.1002/pro.3235.
- Casañal, A., Lohkamp, B., and Emsley, P. (2020). Current developments in Coot for macromolecular model building of Electron Cryo-microscopy and Crystallographic Data. Protein Sci. 29, 1069–1078. https://doi.org/10. 1002/pro.3791.
- Afonine, P.V., Poon, B.K., Read, R.J., Sobolev, O.V., Terwilliger, T.C., Urzhumtsev, A., and Adams, P.D. (2018). Real-space refinement in PHENIX for cryo-EM and crystallography. Acta Crystallogr. D Struct. Biol. 74, 531–544. https://doi.org/10.1107/S2059798318006551.
- Schindelin, J., Arganda-Carreras, I., Frise, E., Kaynig, V., Longair, M., Pietzsch, T., Preibisch, S., Rueden, C., Saalfeld, S., Schmid, B., et al. (2012). Fiji: an open-source platform for biological-image analysis. Nat. Methods 9, 676–682. https://doi.org/10.1038/nmeth.2019.
- Waterhouse, A.M., Procter, J.B., Martin, D.M.A., Clamp, M., and Barton, G.J. (2009). Jalview Version 2—a multiple sequence alignment editor and analysis workbench. Bioinformatics 25, 1189–1191. https://doi.org/ 10.1093/bioinformatics/btp033.

- Jumper, J., and Hassabis, D. (2022). Protein structure predictions to atomic accuracy with AlphaFold. Nat. Methods 19, 11–12. https://doi. org/10.1038/s41592-021-01362-6.
- 64. Katoh, K., and Standley, D.M. (2013). MAFFT multiple sequence alignment software version 7: improvements in performance and usability. Mol. Biol. Evol. 30, 772–780. https://doi.org/10.1093/molbev/mst010.
- Crooks, G.E., Hon, G., Chandonia, J.M., and Brenner, S.E. (2004).
   WebLogo: a sequence logo generator. Genome Res. 14, 1188–1190. https://doi.org/10.1101/gr.849004.
- Tan, Y.Z., Baldwin, P.R., Davis, J.H., Williamson, J.R., Potter, C.S., Carragher, B., and Lyumkis, D. (2017). Addressing preferred specimen orientation in single-particle cryo-EM through tilting. Nat. Methods 14, 793–796. https://doi.org/10.1038/nmeth.4347.
- UniProt Consortium (2025). UniProt: the Universal Protein Knowledgebase in 2025. Nucleic Acids Res. 53, D609–D617. https://doi.org/10.1093/nar/ gkae1010.
- 68. Parks, D.H., Chuvochina, M., Rinke, C., Mussig, A.J., Chaumeil, P.A., and Hugenholtz, P. (2022). GTDB: an ongoing census of bacterial and archaeal diversity through a phylogenetically consistent, rank normalized and complete genome-based taxonomy. Nucleic Acids Res. 50, D785–D794. https://doi.org/10.1093/nar/gkab776.
- Draizen, E.J., Shaytan, A.K., Mariño-Ramírez, L., Talbert, P.B., Landsman, D., and Panchenko, A.R. (2016). HistoneDB 2.0: a histone database with variants—an integrated resource to explore histones and their variants. Database (Oxford) 2016, baw014. https://doi.org/10.1093/database/baw014.
- Scheres, S.H.W., and Chen, S. (2012). Prevention of overfitting in cryo-EM structure determination. Nat. Methods 9, 853–854. https://doi.org/10. 1038/nmeth.2115.

### **Article**



#### **STAR**\*METHODS

#### **KEY RESOURCES TABLE**

REAGENT or RESOURCE	SOURCE	IDENTIFIER
Bacterial and virus strains		
E.coli BL21 CodonPlus (DE3) RIL	Agilent Technologies	230245
E.coli BL21 LOBSTR (DE3)	Kerafast	EC1002
Chemicals, peptides, and recombinant proteins		
Protease inhibitor cocktail	Roche	4693116001
Kanamycin	Carl Roth	T832.2
IPTG	Carl Roth	367-93-1
Roti Garose-his/Ni NTA-HP beads	Carl Roth	805.1
Glutathione sepharose 4 fast flow beads	Sigma Aldrich	GE17-5132-01
HiTrap SP column	Sigma Aldrich	GE17-1152-01
Phusion Polymerase	NEB	M0530L
Phusion HF Buffer Pack	NEB	B0518S
dNTP Mix (10mM each)	Thermo Fisher Scientific	Cat# R0192
SYBR GOLD nucleic acid stain	Invitrogen	Cat# S11494
Atto647N-maledimide	Jena Biosciences	FP-202-647N
Triton X-100	Sigma Aldrich	CAT# X100-1L
Glycerol	Carl Roth	7530.4
GeneRuler Ultra Low Range DNA Ladder	Thermo Fisher Scientific	SM1213
PD-10 desalting column	Cytiva	Cat# 17085101
Tween-20	Sigma Aldrich	Cat# P7949
Streptavidin coated beads	Lumicks	SKU 11288
Miniprep kit	Qiagen	Cat# 27104
Quantifoil R 2/1 Cu 200 mesh grids	Quantifoil	N/A
Deposited data	4.000.000	
HHoB nucleosome in open state (MAP)	This study	EMD-53390
HHoB open hypernucleosome (MAP)	This study	EMD-53389
HHoB closed hypernucleosome (MAP)	This study	FMD-53387
**	This study This study	EMD-53387 EMD-53386
HHoB nucleosome in closed state in	This study This study	EMD-53387 EMD-53386
HHoB nucleosome in closed state in 1mM MgCl2 (MAP) HHoB nucleosome in open state in	•	
HHoB nucleosome in closed state in 1mM MgCl2 (MAP) HHoB nucleosome in open state in 1mM MgCl2 (MAP)	This study This study	EMD-53386
HHoB nucleosome in closed state in 1mM MgCl2 (MAP) HHoB nucleosome in open state in	This study This study This study	EMD-53386 EMD-53388
HHoB nucleosome in closed state in 1mM MgCl2 (MAP) HHoB nucleosome in open state in 1mM MgCl2 (MAP) HHoB open state model HHoB closed state model	This study This study This study This study	EMD-53386  EMD-53388  PDB: 9QV7
1mM MgCl2 (MAP) HHoB nucleosome in open state in 1mM MgCl2 (MAP) HHoB open state model	This study This study This study	EMD-53386  EMD-53388  PDB: 9QV7 PDB: 9QV5
HHoB nucleosome in closed state in  1mM MgCl2 (MAP)  HHoB nucleosome in open state in  1mM MgCl2 (MAP)  HHoB open state model  HHoB closed state model  HHoB closed hypernucleosome model  Oligonucleotides  6-FAM-Labeled 33 nucleotide DNA oligo  (AGGGTCACATGGGTGTTTTGGCACTAC	This study This study This study This study	EMD-53386  EMD-53388  PDB: 9QV7 PDB: 9QV5
HHoB nucleosome in closed state in  1mM MgCl2 (MAP)  HHoB nucleosome in open state in  1mM MgCl2 (MAP)  HHoB open state model  HHoB closed state model  HHoB closed hypernucleosome model  Oligonucleotides  6-FAM-Labeled 33 nucleotide DNA oligo (AGGGTCACATGGGTGTTTGGCACTAC CGACAGT-6-FAM)	This study This study This study This study This study	EMD-53386  EMD-53388  PDB: 9QV7  PDB: 9QV5  PDB: 9QV6
HHoB nucleosome in closed state in  1mM MgCl2 (MAP)  HHoB nucleosome in open state in  1mM MgCl2 (MAP)  HHoB open state model  HHoB closed state model  HHoB closed hypernucleosome model  Oligonucleotides  6-FAM-Labeled 33 nucleotide DNA oligo (AGGGTCACATGGGTGTTTGGCACTAC CGACAGT-6-FAM)  Unlabeled 33 nucleotide DNA oligo ACTG	This study This study This study This study This study IDT DNA	EMD-53386  EMD-53388  PDB: 9QV7  PDB: 9QV5  PDB: 9QV6
HHoB nucleosome in closed state in  1mM MgCl2 (MAP)  HHoB nucleosome in open state in  1mM MgCl2 (MAP)  HHoB open state model  HHoB closed state model  HHoB closed hypernucleosome model  Oligonucleotides  6-FAM-Labeled 33 nucleotide DNA oligo (AGGGTCACATGGGTGTTTGGCACTAC CGACAGT-6-FAM)  Unlabeled 33 nucleotide DNA oligo ACTG TCGGTAGTGCCAAACACCCATGTGACCCT	This study This study This study This study This study IDT DNA	EMD-53386  EMD-53388  PDB: 9QV7  PDB: 9QV5  PDB: 9QV6
HHoB nucleosome in closed state in  1mM MgCl2 (MAP)  HHoB nucleosome in open state in  1mM MgCl2 (MAP)  HHoB open state model  HHoB closed state model  HHoB closed hypernucleosome model  Oligonucleotides  6-FAM-Labeled 33 nucleotide DNA oligo (AGGGTCACATGGGTGTTTGGCACTAC CGACAGT-6-FAM)  Unlabeled 33 nucleotide DNA oligo ACTG TCGGTAGTGCCAAACACCCATGTGACCCT  Recombinant DNA  Plasmid: pETHis6TEVLic1B	This study This study This study This study This study IDT DNA	EMD-53386  EMD-53388  PDB: 9QV7  PDB: 9QV5  PDB: 9QV6
HHoB nucleosome in closed state in  1mM MgCl2 (MAP)  HHoB nucleosome in open state in  1mM MgCl2 (MAP)  HHoB open state model  HHoB closed state model  HHoB closed hypernucleosome model  Oligonucleotides  6-FAM-Labeled 33 nucleotide DNA oligo (AGGGTCACATGGGTGTTTGGCACTAC  CGACAGT-6-FAM)  Unlabeled 33 nucleotide DNA oligo ACTG TCGGTAGTGCCAAACACCCATGTGACCCT  Recombinant DNA	This study This study This study This study This study IDT DNA IDT DNA Addgene	EMD-53386  EMD-53388  PDB: 9QV7  PDB: 9QV5  PDB: 9QV6  N/A  N/A  Cat# 29653
HHoB nucleosome in closed state in  1mM MgCl2 (MAP)  HHoB nucleosome in open state in  1mM MgCl2 (MAP)  HHoB open state model  HHoB closed state model  HHoB closed hypernucleosome model  Oligonucleotides  6-FAM-Labeled 33 nucleotide DNA oligo (AGGGTCACATGGGTGTTTGGCACTAC CGACAGT-6-FAM)  Unlabeled 33 nucleotide DNA oligo ACTG TCGGTAGTGCCAAACACCCATGTGACCCT  Recombinant DNA  Plasmid: pETHis6TEVLic1B  Plasmid: pETHis6TEVLic1B-HHoB  Plasmid: pETHis6TEVLic1B-HHoF	This study This study This study This study This study IDT DNA IDT DNA Addgene This study	EMD-53386  EMD-53388  PDB: 9QV7  PDB: 9QV5  PDB: 9QV6  N/A  N/A  Cat# 29653  N/A
HHoB nucleosome in closed state in  1mM MgCl2 (MAP)  HHoB nucleosome in open state in  1mM MgCl2 (MAP)  HHoB open state model  HHoB closed state model  HHoB closed hypernucleosome model  Oligonucleotides  6-FAM-Labeled 33 nucleotide DNA oligo (AGGGTCACATGGGTGTTTGGCACTAC CGACAGT-6-FAM)  Unlabeled 33 nucleotide DNA oligo ACTG TCGGTAGTGCCAAACACCCATGTGACCCT  Recombinant DNA  Plasmid: pETHis6TEVLic1B  Plasmid: pETHis6TEVLic1B-HHoB	This study This study This study This study This study IDT DNA IDT DNA Addgene This study This study	EMD-53386  EMD-53388  PDB: 9QV7 PDB: 9QV5 PDB: 9QV6  N/A  N/A  Cat# 29653 N/A N/A

(Continued on next page)



Continued		
REAGENT or RESOURCE	SOURCE	IDENTIFIER
Plasmid: pETIDT-HHoBMut2	IDT	N/A
Plasmid: pETHis6TEVLic1B-HHoB-GGGC	This study	N/A
Plasmid: pMA/pMK-420bp	GeneArt	N/A
Plasmid: pMA/pMK-147bp_Wid601	GeneArt	N/A
Biotinylated Lambda DNA	Lumicks	SKU 00001
Software and algorithms		
SerialEM	University of Colorado Boulder <sup>57</sup>	https://bio3d.colorado.edu/SerialEM/
cryoSPARC v4.4.1	Punjani et al. <sup>33</sup>	https://cryosparc.com/
UCSF ChimeraX v.1.7.1	Goddard et al. <sup>58</sup>	https://www.rbvi.ucsf.edu/chimerax/
Coot v0.9.8.93 EL	Casañal et al. <sup>59</sup>	https://www2.mrc-lmb.cam.ac.uk/ personal/pemsley/coot/
ISOLDE v1.3	Croll <sup>36</sup>	https://isolde.cimr.cam.ac.uk/
Phenix v1.21.1	Afonine et al. <sup>60</sup>	https://phenix-online.org/
FIJI v2.16.0	Schindelin et al. <sup>61</sup>	https://imagej.net/software/fiji/
JASP v0.19.3	JASP team	https://jasp-stats.org
Python + Pylake v1.6.1	LUMICKS	DOI https://doi.org/10.5281/zenodo.4280788
Jalview v2.11.4.1	Waterhouse et al. <sup>62</sup>	https://www.jalview.org
Alphafold2	Jumper and Hassabis <sup>63</sup>	https://github.com/google-deepmind/alphafold
MO.AffinityAnalysis	NanoTemper Technologies GmbH	http://www.nanotempertech.com
MAFFT v7	Katoh K and Stankley <sup>64</sup>	https://mafft.cbrc.jp
Weblogo v2.8.2	Crooks et al.65	https://weblogo.berkeley.edu
Other		
Monolith NT.115 MST Premium Coated Capillaries	NanoTemper Technologies	K005

#### **EXPERIMENTAL MODEL AND STUDY PARTICIPANT DETAILS**

#### **Plasmids and strains**

Full-length histone sequences from Asgard genome Hodarchaeaota LC\_3 (GCA\_001940645.1) were codon-optimised for expression in *E. coli*, and then incorporated into the LIC 1B plasmid from MacroLabs (pET His6 TEV LIC cloning vector 1B - Addgene #29653). Accordingly, the HHoB histone (Uniprot A0A1Q9NRY6, 7.5 kDa) expression construct in a LIC 1B vector contained an N-terminal 6×His-tag followed by a tobacco etch virus (TEV) protease cleavage site.

Histones HHoF (Uniprot A0A1Q9N8N6, 7.7 kDa), HHoG (Uniprot A0A1Q9NAM9, 7.9 kDa) and HMfB from *Methanothermus fervidus* (Uniprot P19267, 7.7 kDa) were also incorporated into LIC 1B expression plasmids.

#### **METHOD DETAILS**

#### **HHoB** mutagenesis

Mutants of HHoB were generated as follows. The specific mutations introduced were as follows: HHoB mut1 (Y44A I48Y); HHoB mut2 (K29A E32A D36A); and HHoB-Atto647N, which included a wild-type HHoB with additional GGGC at the C-terminus (later used for labelling). Constructs for mut1 and mut2 were ordered from IDT as part of a pET-IDT expression vector. For HHoB-Atto647N, following PCR amplification, the mutant plasmids were transformed into *E. coli* XL-blue cells and screened by colony PCR. Plasmid DNA was extracted using a Miniprep Kit (Qiagen) and the mutations were validated by Sanger sequencing (Eurofins Genomics).

#### **Protein expression and purification**

HHoB, mut1, mut2 and HHoB-Atto647N proteins were expressed in *E. coli* BL21-CodonPLus (DE3)-RIL strain by induction (0.5 mM IPTG at  $OD_{600}$  0.5-0.6) and incubated at 37 °C for 3-4 hours. Cell pellet was harvested by centrifugation at 4000 rpm at 4 °C in and stored at -20 °C. Cell pellets were thawed in lysis buffer containing 20 mM HEPES pH 7.5, 300 mM NaCl, 5 % glycerol, 1 % Triton X-100 and 1x protease inhibitor (PI tablet, Roche) for 20 min at 4 °C. Lysis was further carried out by sonication for 10 min at 30 % power and 0.4 s duty cycle using a Branson sonifier. The cell lysate was centrifuged at 27,000 g for 20 min at 4 °C. The supernatant was collected, and Histagged histone HHoB was enriched using affinity purification using ROTI®Garose-His/Ni NTA-HP beads (Carl Roth). The His-tag was

### **Molecular Cell** Article



cleaved off using GST-tagged TEV protease during overnight dialysis into buffer B (20 mM HEPES pH 7.5, 200 mM NaCl, 5 % glycerol). Protease was removed from the solution using Glutathione Sepharose 4 Fast Flow beads (Cytiva). After a polishing step using cation exchange HiTrap SP column (5 ml, Cytiva) the protein was dialysed back into buffer B. Concentrations were determined using Nanodrop One (Thermo Fischer Scientific). Folding state of the proteins was confirmed using circular dichroism (CD) spectra. Aliquots were snapfrozen in liquid nitrogen and stored at -80 °C. HHoF and HHoF histones from LC\_3 were expressed and purified according to the same protocol as for HHoB histone. HMfB histone (*M. fervidus*) was expressed in *E. coli* LOBSTR cells by induction (0.5 mM IPTG at OD<sub>600</sub> 0.5-0.6) and incubated at 37 °C for 3-4 hours. The purification steps were identical to HHoB, with an additional heat incubation step of the supernatant (after lysis) at 80 °C for 15 mins in a water bath. This helped enriching for the thermostable HMfB histone.

#### **DNA** sequences and preparation

The Widom601<sup>22</sup> derived 147 bp sequence was used for EMSAs and cryoEM:

CTGGAGAATCCCGGTGCCGAGGCCGCTCAATTGGTCGTAGACAGCTCTAGCACCGCTTAAACGCACGTACGCGCTGTCCCCCGCGTTTTAACCGCCAAGGGGATTACTCCCTAGTCTCCAGGCACGTGTCAGATATATACATCCTGT.

A short DNA of random sequence and length 33 bp DNA with 6-FAM on the 3' end: AGGGTCACATGGGTGTTTGGCACT ACCGACAGT-6-FAM was used for Micro-scale thermophoresis (MST). The oligos for the 33 bp were ordered from Sigma (HPLC-purified), and annealed together by heating up to 98 °C, and then were gradually cooled down.

Native LC\_3 sequence (420 bp length) from gene HeimC3\_31310 was used for EMSA and cryo-EM:

DNA constructs were ordered from GeneArt as parts of pMA or pMK vectors. DNA templates of interest were amplified by PCR, and purified via ion exchange (Resource Q column 5 ml, Cytiva). Force spectroscopy measurements were performed using biotinylated double stranded λ DNA of length 48.5 kb (SKU 00001, Lumicks).

#### In-vitro reconstitution and binding affinity measurements

Histone-DNA complexes were reconstituted in reaction buffer containing 20 mM HEPES pH 7.5, 100 mM NaCl, 5 % glycerol. DNA concentration was kept constant (18 nM) and protein concentration was varied (9 – 540 nM). The reaction was incubated for 20 min at RT, then put on ice, and samples were loaded into the wells of a  $5.5 \% 0.5 \times TBE$  PAGE gel. EMSAs were run at 80 V for 90 min in  $0.5 \times TBE$  buffer at  $4 \, ^{\circ}\text{C}$ . EMSA gels were then stained with SYBR gold (Invitrogen) and imaged in a Typhoon FLA  $9500 \, \text{(GE)}$  imager. To study histone-DNA binding in the presence of magnesium ions, the reaction buffer and running buffer were supplemented with  $10 \, \text{mM} \, \text{MgCl}_2$  and EMSAs were run for  $120 \, \text{min}$  at  $80 \, \text{V}$ .

EMSA with DNA substrates of different lengths was done by mixing GeneRuler Ultra Low Range Ladder with HHoB at the indicated w/w ratios in 20 mM HEPES pH 7.5, 100 mM NaCl, 5 % glycerol (with 0 or 10 mM MgCl<sub>2</sub>). Samples were incubated at RT for 30 minutes before being run in 10 % TBE-polyacrylamide gel at 120 V for 60 minutes (105 minutes for samples with MgCl<sub>2</sub>) at 4 °C.

The binding affinity of HHoB was quantified using MST with a random 33 bp DNA oligonucleotide as the substrate. Experiments were conducted using a Monolith NT.115 (NanoTemper Technologies) with "blue" excitation at 40 % LED power. The DNA substrate was used at a final concentration of 15.5 nM. Samples were prepared in a buffer containing 20 mM HEPES (pH 7.5), 100 mM NaCl, and 0.05 % Tween-20, with an additional condition in which the buffer was supplemented with 1 mM MgCl<sub>2</sub>. Measurements were performed in triplicates using Monolith NT.115 MST Premium Coated Capillaries (K005, NanoTemper Technologies). Data were analyzed using the Kd fit model in MO.Affinity analysis software (NanoTemper Technologies).

#### Sample preparation for cryo-EM

Nucleosomes were reconstituted by mixing DNA and histone proteins at a 1:20 molar ratio (DNA concentration 1.9  $\mu$ M) in buffer A containing 20 mM HEPES (pH 7.5) and 100 mM NaCl. For magnesium concentration screening, nucleosome reconstitution was performed in buffer A supplemented with 1, 20, 40, 60, 80, or 100 mM MgCl<sub>2</sub>. Samples were incubated at room temperature (RT) for 20 min and subsequently placed on ice until plunge-freezing. Cryo-EM grid preparation was performed using Quantifoil R 2/1 Cu 200 mesh grids, which were glow-discharged for 20 s at 0.26 mbar pressure and 25 mA current using a PELCO easiGlow (Ted Pella) device. A 3  $\mu$ l aliquot of the sample was applied to the grids inside a Vitrobot Mark IV (Thermo Fisher Scientific) at 100 % humidity and 20 °C. Excess liquid was blotted away with a blot force of 7 for 2.5 s, and the grids were vitrified by plunging into liquid ethane.

#### **Data collection**

Data collection of HHoB – DNA complex in buffer A was performed on a 300 kV Titan Krios microscope (FEI) with a K2 summit direct electron detector (Gatan) in counting mode. A quantum energy filter (Gatan) was used with a slit width set to 20 eV. 3660 movies were collected with Serial EM software,  $^{57}$  with defocus ranging from -1.5 to -2.5  $\mu m$  at a nominal magnification of 130 kx and a pixel size of 1.04 Å. A constant stage tilt of 25° was applied during acquisition in order to compensate for "preferred" orientation of the particles. The total electron dose of 46.63 e $^-/\mathring{\rm A}^2$  was distributed over 40 frames. At the same microscope, datasets were also collected for the



### Molecular Cell Article

magnesium screen – these involved micrographs for samples in 20 mM, 40 mM, 60 mM and 80 mM MgCl<sub>2</sub>, taken with the same acquisition parameters of 65.04  $e^-/\text{Å}^2$  dose, 130kx magnification and defocus range of -0.5 to -1.75  $\mu$ m. Data Collection for HHoB mut1 and HHoB mut2 in 1 mM and 100 mM MgCl<sub>2</sub> respectively were also carried out on the same microscope. HHoB mut1 dataset was collected at 130 kx magnification and pixel size of 1.04 Å. A dose of 62.44  $e^-/\text{Å}^2$  was spread over 40 frames. HHoB mut2 dataset was collected at 105 kx magnification and pixel size of 1.33 Å. A dose of 51.87  $e^-/\text{Å}^2$  and this was distributed over 35 frames. The defocus range in both these datasets was -0.5 to -1.75  $\mu$ m.

Data collection of HHoB – DNA complex in buffer containing 1 mM MgCl<sub>2</sub> was performed on a G4 Titan Krios microscope (FEI) equipped with a Falcon4i direct electron detector (Thermo Fischer Scientific) and Selectris X Energy filter. Data were collected with Serial EM software,  $^{57}$  with defocus ranging from -0.5 to -1.75  $\mu$ m at a nominal magnification of 165 kx and a pixel size of 0.73 Å. Energy filter slit width was set to 20 eV. The total electron dose of 59.44 e<sup>-</sup>/Å<sup>2</sup> was distributed over 40 movie frames recorded in EER format.

Micrographs of HHoB – DNA complex in buffer A supplemented with 20 mM MgCl $_2$  were recorded on a 300 kV Titan Krios microscope with a K3 detector and Quantum energy filter. Data were collected with SerialEM software, with a defocus range of -0.5 to -1.5  $\mu$ m at 105 kx magnification and pixel size of 0.82 Å. The width of the energy filter was set to 20 eV with a total electron dose of 63.84 e $^-$ /Å $^2$ . This was distributed over 40 frames. Micrographs for processing HHoB in 100 mM MgCl $_2$  were collected on the same microscope, with a defocus range of -0.5 to -1.5  $\mu$ m at 130 kx magnification and pixel size of 0.645 Å. The width of the energy filter was set to 20 eV with a total electron dose of 39.93 e $^-$ /Å $^2$ . This dose was distributed over 40 frames.

#### **Data processing and analysis**

Data processing for all datasets was carried out in cryoSPARC<sup>33</sup> (v.4.4.1).

#### Dataset 1 (buffer A - no MgCl<sub>2</sub>)

After preprocessing, 4,300 particle picks were curated from a blob picker by 2D classification and Topaz<sup>39</sup> model was trained using these particles – they were used for picking particles from the entire dataset and another topaz model was trained on these picks after 2D classification. 318,063 particles were then used for 2D classification to eliminate junk particles, and followed by ab-initio reconstruction, and 3D classification into 3 classes. One well-resolved class was then selected, and it contained 96,361 particles. The map was processed by non-uniform refinement and per-particle CTF correction to yield the final map at 4.4 Å. 3DFSC server<sup>66</sup> was used to ensure isotropic resolution of the structures.

#### Dataset 2 (buffer A + 1 mM MgCl<sub>2</sub>)

After preprocessing, 50k particles were curated after blob and template picking. The dataset showed preferred orientation for top views, and large heterogeneity in conformations, so two topaz models were trained – one for top views and another for side and oblique views. In total, 3,108,514 particles were picked and filtered through two rounds of 2D classifications into open and closed conformations. Then ab-initio reconstruction and 3D classification (into 2 classes each) for open and closed conformations were performed separately. Good classes (96,738 particles for open and 117,260 particles for closed conformation) were processed by non-uniform refinement and post processed by CTF and reference-based motion correction to yield the final maps at 3.6 Å and 3.5 Å for the open and closed conformation respectively. Additionally, 546,206 particles were aligned in 3D by homogenous refinement to a low-resolution mixed conformation. This was subjected to 3D classification to obtain low resolution maps of a range of mixed conformations – highlighting the heterogeneity of the dataset (Figure S4).

#### Dataset 3 (buffer A + 20 mM MgCl<sub>2</sub>)

After preprocessing, 7,816 particle picks were curated from a blob picker by 2D classification and Topaz model was trained using these particles – they were used for picking particles from the entire dataset and another topaz model was trained on these picks after 2D classification. 214,840 particles were then used for 2D classification to eliminate junk particles, followed by ab-initio reconstruction and 3D classification, which resulted in one well-resolved class containing 40,918 particles. From the micrographs and 2D classes it can be appreciated that the dataset indeed contained open hypernucleosomes that are very flexible and contain mixed conformations. The map was processed by non-uniform refinement and per-particle CTF corrections to yield the final map at 10.5 Å. **Dataset 4 (buffer A + 100 mm MgCl<sub>2</sub>)** 

After pre-processing, 4,964,843 particles were picked using filament tracer. After three rounds of 2D classification 484,756 particles were selected for ab initio volume generation and refinements. Initially a cylinder with outer and inner diameter 13 nm and 1 nm respectively was used as template for refinement without helical parameters. Symmetry search was performed and used for helical refinement. The particles were then 3D classified and the well-resolved class (353,468 particles) was helically refined with non-uniform refinement enabled. After per group CTF refinement and reference-based motion correction, final helical refinement was carried out to obtain the HHoB closed hypernucleosome map at 2.6 Å. During helical refinement step in CryoSparc, the helical twist was measured to be 77.9°, rise - 19.4 Å, and pitch - 89.6 Å respectively. Note the symmetry order 3.

#### Dataset 5 (magnesium concentration screen)

Thirty micrographs from the  $40 \, \text{mM} \, \text{MgCl}_2$  dataset were pre-processed and evenly divided into two subsets. Each subset was used to train a separate Topaz model following blob-picking and 2D classification. These independently trained models were then applied to pick particles from 30 micrographs collected at 20, 40, 60, and 80 mM MgCl<sub>2</sub>, as well as from 30 micrographs randomly selected from the 0, 1, and 100 mM MgCl<sub>2</sub> larger datasets. We note, that the 1 mM dataset was collected at a 0.73 Å pixel size, the 100 mM at 0.64 Å pixel size, and the rest (0, 20, 40, 60, 80) at 1.04 Å pixel sizes. The particle box extraction was adjusted accordingly. Following particle picking, all particles underwent 2D classification to remove junk particles and enhance data quality. After this filtering step, the total

### **Molecular Cell** Article



number of particles per dataset ranged from 1,349 to 7,575 (see Table in the Figure S4B). Particles were categorized into open, mixed, or closed conformations based on their 2D class averages. Representative 3D reconstructions of these conformational states, derived from the larger 1 mM MgCl<sub>2</sub> dataset (dataset 2), are presented in Figure S4. Fast Fourier Transform (FFT) analyses of the micrographs (power spectra shown in Figures S5 and S10) were performed using FFT function in FIJI software<sup>61</sup> (version 2.16.0).

#### Model fitting and refinement

Initially, the AlphaFold2 prediction of the histone HHoB dimer was used for rigid body fitting in UCSF ChimeraX<sup>58</sup> v.1.7.1. After real space refinement in Phenix<sup>60</sup> (v1.21.1), per residue fitting was done in Coot<sup>59</sup> v 0.9.8.93 EL using all-molecule self-restraints and finally the model was relaxed into the density using ISOLDE<sup>36</sup> in ChimeraX. For the open conformation model, DNA was fit into the densities by ISOLDE relaxation from H3-H4 open eukaryotic octasome structure (PDB: 7X58<sup>12</sup>) with DNA H-bond restraints. For the closed conformation, the same procedure was performed using DNA from the eukaryotic nucleosome structure (PDB: 1AOI). Nucleic acid backbone angles were refined with DNA B-form restraints in Coot. RMSD and surface area calculations were performed in ChimeraX. For RMSD we report all values with the 0.1 Å, however, we note that in the resolution regime that we operate at (2.6-3.6 Å) the error in the C $\alpha$  atom positioning might be slightly higher than 0.1 Å.

#### Protein labelling with fluorescent dye

To label HHoB-Atto647N, it was incubated at molar ratio 1:5 with Atto647N-maleimide (FP-202-647N, Jena Biosciences) overnight at RT on a shaker in buffer A. Free dye was removed from buffer using desalting column (PD-10, Cytiva). The degree of labeling was estimated with the Nanodrop (Thermo Fisher Scientific) to be 0.99 (99 %). Aliquots were snap frozen in liquid nitrogen and stored at -80 °C. DNA binding properties of labelled HHoB were the same as for unlabelled according to EMSA (data not shown).

#### Force Spectroscopy measurement and analysis

Single-molecule force-extension measurements were performed using a high-resolution correlative fluorescence optical tweezers instrument (C-trap, LUMICKS). A microfluidic flow cell (LUMICKS) with five parallel laminar flow channels was used, allowing the controlled movement of the optical traps between different solutions. Streptavidin-coated polystyrene beads (4.35  $\mu$ m in diameter) were trapped in phosphate-buffered saline (1xPBS) and used to anchor biotinylated double-stranded  $\lambda$  DNA (48.5 kb) for force measurements. The traps were calibrated to have a stiffness of 0.3 to 0.4 pN/nm. The first baseline measurement was taken prior to DNA anchoring in the buffer channel containing Buffer C (20 mM HEPES pH 7.5, 100 mM NaCl, 0.1 % BSA). Force-extension measurements were performed by stretching the DNA from a low-force regime (L= 8  $\mu$ m) to a high-force, stretched state (L= 16.7  $\mu$ m) at a pulling speed of 0.5  $\mu$ m/s. Following this, the anchored DNA was incubated in the protein channel containing 200 nM histone in the same buffer for 5 minutes at an inter-bead distance of 8  $\mu$ m. Force-extension measurements were then performed on the histone-DNA complex by stretching from the relaxed to stretched state at a pulling speed of 0.05  $\mu$ m/s. After histone incubation and force-extension measurements, the DNA was ruptured by further bead separation to ensure complete removal, and a second baseline measurement was recorded in the protein-containing channel. The first baseline was used to correct force-extension data for free DNA, while the second was used to correct for the histone-DNA complex. All data were processed and analyzed in Python using the LUMICKS Pylake library (version 1.6.1). Statistical comparisons were performed using paired t-tests in JASP (version 0.19.3) to assess force differences between datasets.

#### **Tethered Particle Motion**

Tethered Particle Motion (TPM) experiments were done following the procedure described in <sup>14</sup> on a 685 bp DNA substrate with a 47 % GC content in 20 mM HEPES, pH 7.5, 200 mM NaCl, 5 % glycerol. Each measurement was done in duplicate. To select for single-tethered beads, an anisotropic ratio cutoff of 1.3 and a standard deviation cut-off of 8 % were used. Data analysis was done as described in Henneman et al. (2024). <sup>44</sup> The end-to-end distance was calculated by subtracting the mean bead radius from the largest 5 % XY-displacement of all beads in each measurement.

#### **Multi-Sequence Alignment**

The histone sequences were obtained from recent studies <sup>16,48,64</sup> and Uniprot. <sup>67</sup> Their respective UniProt IDs are mentioned in Figure S12. Overall, 2126 archaeal histones were aligned using MAFFT, <sup>64</sup> then cross-referenced with the GTDB <sup>68</sup> taxonomy database to classify into Euryarchaeal (673 sequences), Asgard (684 sequences), and a subset of Asgard lineages closest to eukaryotes (138 sequences). Additionally, 2000 canonical eukaryotic histoen H4 sequences were obtained from Histone DB (v 2.0). <sup>69</sup> Software JalView <sup>62</sup> (v 2.11.4.1) was used for visualization and sequence logos were generated using WebLogo <sup>65</sup> (v2.8.2).

#### **QUANTIFICATION AND STATISTICAL ANALYSIS**

For cryo-EM structure determination, the numbers of particles used for each of the 3D reconstructions or for open vs close state quantifications are listed in Table 1, or in Figure S4B.

Fourier Shell Correlation (FSC) analyses for resolution determination were performed in cryoSPARC according to standard procedures.<sup>70</sup>